

Pulsar radio emission mechanism II. On the origin of relativistic Langmuir solitons in pulsar plasma

Sk. Minhajur Rahaman,¹★ Dipanjan Mitra,^{1,2} George I. Melikidze,^{2,3} Taras Lakoba⁴

¹*National Centre for Radio Astrophysics, Tata Institute of Fundamental Research, Post Bag 3, Ganeshkind, Pune-411007, INDIA*

²*Janusz Gil Institute of Astronomy, University of Zielona Góra, ul Szafrana 2, 65-516 Zielana Góra, Poland*

³*Abastumani Astrophysical Observatory, Ilia State University, 3-5 Cholokashvili Ave., Tbilisi, 0160, Georgia*

⁴*Department of Mathematics and Statistics, University of Vermont, Burlington VT 05401, USA*

Accepted XXX. Received YYY; in original form ZZZ

ABSTRACT

Observations suggest that coherent radio emission from pulsars is excited in a dense pulsar plasma by curvature radiation from charge bunches. Numerous studies propose that these charge bunches are relativistic charge solitons which are solutions of the non-linear Schrödinger equation (NLSE) with a group velocity dispersion (G), cubic-nonlinearity (q) and non-linear Landau damping (s). The formation of stable solitons crucially depends on the parameters G , q and s and the particle distribution function. In this work, we use realistic pulsar plasma parameters obtained from observational constraints to explore the parameter space of NLSE for two representative distribution functions (DF) of particles' momenta: Lorentzian (long-tailed) and Gaussian (short-tailed). The choice of DF critically affects the value of $|s/q|$, which, in turn, determines whether solitons can form. Numerical simulations show that well-formed solitons are obtained only for small values of $|s/q| \lesssim 0.1$ while for moderate and higher values of $|s/q| \gtrsim 0.5$ soliton formation is suppressed. Small values for $|s/q| \sim 0.1$ are readily obtained for long-tailed DF for a wide range of plasma temperatures. On the other hand, short-tailed DF provides these values only for some narrow range of plasma parameters. Thus, the presence of a prominent high-energy tail in the particle DF favours soliton formation for a wide range of plasma parameters. Besides pair plasma, we also include an iron ion component and find that they make a negligible contribution in either modifying the NLSE coefficients or contributing to charge separation.

Key words: waves – plasmas – pulsars: general – radiation mechanisms: non-thermal – relativistic processes.

1 INTRODUCTION

Understanding the mechanisms of coherent radio emission from pulsars has been a challenging astrophysical problem since the discovery of pulsars. Most models of coherent radio emission involve growth of instability in strongly magnetized relativistically streaming pair plasma and are broadly classified into maser or antenna mechanisms (see e.g. [Ginzburg et al. 1969](#); [Kazbegi et al. 1991](#); [Melrose 1995](#)). Recent single pulse polarization observations, however, strongly favour the antenna mechanism, where the radio emission is excited in pair plasma by coherent curvature radiation (hereafter CCR) due to motion of charge bunches along curved magnetic field lines ([Mitra et al. 2009](#)).

Observations have further established that the radio emission detaches the pulsar magnetosphere from around 500 km above the neutron star surface ([Kijak & Gil 1997](#); [Kijak & Gil 1998](#); [Mitra 2017](#)), where the magnetic field topology is purely dipolar ([Mitra & Li 2004](#)). At the

★ E-mail: rahaman.minhajur93@gmail.com

radio emission region, due to enormously strong magnetic field, the motion of plasma particles can be approximated to be one-dimensional. The primary source of pair plasma in pulsars is due to magnetic pair production by high energy photons at the polar cap. In our study we consider the scenario for $\vec{\Omega}_{\text{Rot}} \cdot \vec{B} < 0$ in which a charge-starved inner accelerating region (IAR) region develops above the polar cap where unscreened electric field exists and the primary pairs are formed and accelerated to extremely high Lorentz factors γ_p (see [Sturrock 1971, RS75](#)). One kind of charges is accelerated away from the polar cap, and these charges can radiate high energy photons, which in turn produces a cascade of secondary pair plasma moving with Lorentz factor γ_s . Several lines of evidence suggest a strongly non-dipolar magnetic field topology at the surface ([Geppert 2017](#); [Arumugasamy & Mitra 2019](#); [Mitra et al. 2020](#)) and in such strong fields copious pair creation can occur. As a result, dense and hot pair plasma is produced. The density of the pair plasma exceeds the co-rotation Goldreich-Julian charge density ([Goldreich & Julian 1969](#)) by a factor $\kappa \sim 10^4 - 10^5$ ([Arendt & Eilek 2002](#)), streaming with a bulk Lorentz factor $\gamma_s \approx 10^2 - 10^3$ in the observer's frame of reference. Observations of Pulsar Wind nebulae has also confirmed the presence of a dense pair plasma ([Blasi & Amato 2011](#)). In the IAR, the charge which accelerates towards the polar cap can heat the polar cap to high temperatures, and X-ray observation have revealed the presence of such hot polar cap in several pulsars. However, extremely high temperatures could be expected if the polar cap discharges were to occur under pure vacuum conditions, which is not observed. Hence to properly account for the polar cap temperature, [Gil et al. \(2003\)](#) suggested that the IAR is a Partially Screened Gap (PSG). The PSG model is a variant of the pure vacuum models and takes into consideration the binding energy of iron ions on the surface. The heating due to backflowing charges unpins iron ions from the surface and contributes close to 90 % of the co-rotational charge density. The flow of ions is thermostatically regulated as follows: if the surface is heated beyond some critical temperature T_{ion} , the gap closes completely while for surface temperature below T_{ion} the gap is partially screened. Under equilibrium conditions, the surface temperature is only slightly offset from the critical temperature and any greater offset is corrected on timescales of few hundred nanoseconds. Owing to a heavier mass, the iron ions are accelerated to Lorentz factors γ_{ion} close to the Lorentz factor of the secondary plasma γ_s . The PSG model is a very successful phenomenological model for explaining the subpulse drift rates, mode changing and thermal X-ray luminosity (see e.g. [Basu et al. 2016](#); [Rahaman et al. 2021](#); [Szary et al. 2015](#)). The presence of an additional iron component in the pulsar plasma is hence an important ingredient. To summarize, magnetically induced pair cascades and outflow of ions above the polar cap gives rise to an ultra-relativistic, collisionless and multi-component plasma outflow strictly along the open magnetic field lines of the pulsar ([Goldreich & Julian 1969](#); [Sturrock 1971](#); [Ruderman & Sutherland 1975](#) hereafter RS75).

On the theoretical front, the formation of stable charge bunches capable of explaining coherent radio emission from pulsars has been a long standing puzzle ([Ginzburg et al. 1969](#); [Melrose & Gedalin 1999](#)). Earlier studies suggested that in the radio emission zone linear Langmuir waves can be unstable due to plasma two-stream instability, and as a result, linear charge bunches can radiate coherently (RS75; [Cheng & Ruderman 1977](#)). However, it was soon realised that the very high-frequency linear Langmuir waves disperse the linear bunch well before it can emit coherently ([Lominadze et al. 1986](#); [Melrose & Gedalin 1999](#); [Melikidze et al. 2000](#) hereafter MGP00; [Lakoba et al. 2018](#)). In order to circumvent this problem, studies like that of [Karpman et al. 1975](#); [Melikidze & Pataraya 1980](#); [Pataraya & Melikidze 1980](#); [Melikidze & Pataraya 1984](#); MGP00 explored the non-linear regime of Langmuir waves to provide a time-stable charge distribution. A necessary condition for exploring the non-linear regime is the presence of strong plasma turbulence in the linear regime, and [Asseo & Melikidze \(1998\)](#) and more recently [Rahaman et al. \(2020\)](#) (hereafter Paper I) showed that very effective two-stream instabilities can provide this condition within 1000 km from the neutron star surface. Recent particle-in-cell simulations by [Manthei et al. \(2021\)](#) also established the presence of strong Langmuir turbulence in pulsar plasma. In the non-linear regime the linear Langmuir waves with frequency ω_1 interact to produce low-frequency beats ($\Delta\omega \ll \omega_1$) that modulates the envelope E of the high-frequency linear Langmuir waves. Since the linear waves do not maintain a definite phase relationship with each other over the spatial scale. As a result, the envelope electric field E itself has a white-noise character and the initial envelope electric field is assumed to be completely disordered. The envelope E is governed by the non-linear Schrödinger equation (hereafter NLSE) with a non-local term (see e.g. [Melikidze & Pataraya 1980](#); [Pataraya & Melikidze 1980](#); [Melikidze & Pataraya 1984](#); [Melikidze et al. 2000](#)):

$$i\partial_t E + G\partial_{xx}^2 E + q|E|^2 E + s \mathcal{P} \int dx' V(x, x') = 0. \quad (1)$$

The term $G\partial_{xx}^2 E$ represents the group velocity dispersion (hereafter GVD) of the linear Langmuir waves. The term $q|E|^2 E$ represents cubic non-linearity (hereafter CNL). The non-local term $s \mathcal{P} \int dx' V(x, x')$ represents the non-linear Landau damping (hereafter NLD). NLD represents a resonant interaction at the group velocity of the Langmuir waves with plasma particles. The interaction at group velocity not only gives rise to NLD but also modifies CNL. The coefficient q represents the strength of local (in space) non-linear interactions. The coefficient s represents a non-local interaction via a cascade of energy from higher length scales (lower wave numbers) to shorter length scales (higher wave numbers) (see subsection 3.3). The time-stable solution of Eq. (1) are referred to as solitons, which are considered as candidates for charge bunches giving rise to CCR at radio wavelengths.

In the absence of NLD, Eq. (1) represents a purely local NLSE. [Lighthill \(1967\)](#) showed that this equation admits analytical solutions as solitons, provided that the so-called Lighthill condition represented as

$$Gq > 0, \quad (2)$$

is satisfied and the initial electric wave field is a phase-coherent plane wave. Previous studies by [Melikidze & Pataraya 1978](#); [Melikidze & Pataraya 1980](#); [Pataraya & Melikidze 1980](#); [Melikidze & Pataraya 1984](#); MGP00; neglected NLD to get analytical solutions and conjectured

that the Lighthill condition can be satisfied in pulsar pair plasma. Lakoba et al. (2018) (hereafter LMM18) pursued numerical solution of Eq. (1) and confirmed a previously known fact that purely cubic NLSE cannot give rise to long-living solitons from either an initially disordered electric field E (the most natural state for the Langmuir envelope) or even from a phase-coherent plane wave-like initial electric field. More importantly, LMM18 found that for finite but sufficiently weak non-locality of the nonlinear interactions, i.e., for finite but small values of $|s/q|$, formation of long-living solitons did occur. LMM18 estimated a range of $|s/q|$ values where such formation takes place, but did not address the question whether that range values of $|s/q|$ could actually exist under generic hot plasma conditions in pulsar magnetosphere. Answering it requires modelling of group velocity interaction of Langmuir waves with plasma particles, which depends on the choice of particle momentum distribution function (hereafter DF). Therefore, for such modelling, one needs to consider physically motivated and representative forms of DF in pulsar plasma. To our knowledge, this has not been done in any previous studies and thus has been an open issue.

In order to obtain solitons that can have properties of a charge bunch, the electron-positron DFs of the pair plasma must separate to create charge-separated structures in the configuration space. These charge-separated structures have been proposed as candidates for CCR charge bunches. MGP00 also suggested that the presence of heavier ion species, that had been proposed by the PSG model, can also aid in charge separation. However, the relative contribution of the two effects has not been studied before. Thus, the presence of ions is an important ingredient that has not been considered in earlier studies and hence also needs to be explored.

The present study is focused on addressing the two open issues stated above. Namely, it has the following objectives. Firstly, we want to estimate the ratio of s/q and explore the parameter space for pulsar plasma DFs and then simulate numerically the soliton profiles for the s/q range obtained. Secondly, we want to estimate the relative contribution of the separation of the electron-positron DF and the presence of ions in determining the charge separation in soliton profiles.

The paper is organized as follows. We introduce the NLSE in section 2. The parameter space and soliton solutions of NLSE is explored in section 3. Typical estimates of the charge separation of the Langmuir solitons are presented in section 4. Our conclusions are summarized in section 5.

2 INTRODUCTION TO NLSE WITH NLD

We identify three frames of reference. We have a plasma frame of reference (hereafter PFR) where the average velocity of the pair plasma particles is zero. The PFR moves with a Lorentz factor γ_s with respect to the observer frame of reference (OFR). The moving frame of reference (MFR) moves with respect to PFR at the group velocity of the linear Langmuir waves v_{gr} in PFR. Quantities in MFR are primed while the quantities in PFR are unprimed. The envelope (E) of the Langmuir waves is governed by the NLSE with the NLD,

$$i \frac{\partial E}{\partial \tau'} + G \frac{\partial^2 E}{\partial \xi'^2} + q E |E|^2 + s \frac{1}{\pi} \mathcal{P} \int_{-\infty}^{+\infty} d\xi'' \frac{|E(\xi'', \tau')|^2}{\xi' - \xi''} E = 0, \quad (3)$$

where the quantities τ' and ξ' represents the slow time and space variables in MFR respectively (see Eq. A1 and Eq. A2 in Appendix A). It must be noted that while the equation itself is written in MFR, the coefficients (G, q, s) are computed in PFR. Here the symbol \mathcal{P} stands for the Principal value Cauchy integral.

A complete formal derivation of Eq. (3) is found in Appendix A. Eq. (3) was derived by MGP00 (see also Melikidze & Pataraya 1980; Pataraya & Melikidze 1980; Melikidze & Pataraya 1984), however our derivation differs from MGP00 in one crucial aspect. It allows contributions for arbitrary species of mass m_α and charge e_α (in particular, ions) to be taken into account, while the original derivation of MGP00 was for an electron-positron plasma. Inclusion of ions as an additional plasma component and evaluation of their contribution to the coefficients of the NLSE (3) is one of the stated goals of this study. It must also be noted that in our derivation, certain integrals where MGP00 missed the charge dependencies, have been updated. The setup for the introduction of ions and tracking the charge dependence of multiple species is described in Appendix B.

2.1 The NLSE coefficients

The coefficients of Eq. (3) can be represented in their dimensionless form as (see MGP00, also Eq. B6, B8 and B11 of Appendix B)

$$G = \frac{c^2}{\omega_p^2} (\gamma_{gr}^3 g_d) = \frac{c^2}{\omega_p^2} G_d, \quad (4)$$

$$q = \frac{1}{\omega_p} \left(\frac{e}{m_e c} \right)^2 q_d, \quad (5)$$

$$s = \frac{1}{\omega_p} \left(\frac{e}{m_e c} \right)^2 s_d, \quad (6)$$

where the coefficients (G_d, q_d, s_d) are dimensionless. We will first present an estimate for the plasma frequency ω_p in (4)–(6) and then discuss factors that affect (G_d, q_d, s_d). Values of these coefficients themselves are discussed in the next Section.

The typical plasma frequency at a distance r from the neutron star surface in OFR is

$$\omega_{p,\text{OFR}} = \sqrt{\frac{4\pi n_s e^2}{m_e}} \quad (7)$$

where m_e is the mass of electron, e is charge of electron, $n_s = \kappa B / (Pce)$ is the number density of the pair plasma, κ is the ratio of the number density of the pair plasma to the Goldreich-Julian number density $n_{\text{GJ}} = B / (Pce)$, $B = B_d (r/R_{\text{NS}})^3$ is the magnetic field strength, P is the period of the pulsar, and c is the speed of light. For typical pulsar parameters with period $P = 1$ second, dipolar magnetic field $B_d = 10^{12}$ gauss and radius $R_{\text{NS}} = 10$ km, the corresponding plasma frequency ω_p in PFR can be obtained by the Lorentz transformation to be

$$\omega_p = \frac{\omega_{p,\text{OFR}}}{\gamma_s} \approx 10^8 \left(\frac{200}{\gamma_s} \right) \sqrt{\left(\frac{\kappa}{10^4} \right) \left(\frac{1 \text{ s}}{P} \right) \left(\frac{500 \text{ km}}{r} \right)^3} \text{ rad s}^{-1}, \quad (8)$$

where the Lorentz factor γ_s was discussed in Introduction.

The coefficients (G_d, q_d, s_d) depend only on the plasma particles' momentum distribution function (DF): see Eqs. B7, B9, B12 in Appendix B. Therefore, we now review various relevant models of DF so as to justify its representative forms that we will use in this study. As stated in Introduction, it is well established that normal-period radio pulsars have a strong non-dipolar surface component (see [Arumugasamy & Mitra 2019](#) and the references therein) along with an thermionic ion flow from the surface ([Cheng & Ruderman 1980](#); [Gil et al. 2003](#)). While some semi-analytical estimates of the pair cascade in strong non-dipolar fields have been made ([Szary et al. 2015](#)), the generic shape of the pair plasma DF is not known. However, numerical simulations like those by [Arendt & Eilek \(2002\)](#) show that the shape of the DF is strongly affected by the opening angle between the ambient magnetic field and the initial seed photon, the strength of the magnetic field and the seed photon energy. Namely, for low-opening angles, the DF is well described by the Jüttner-Syngé distribution, so that the number of particles with high dimensionless momenta p (defined in (9)) falls off as $\exp(-K(\ln p/p_0)^2)$, where K is inverse width of the DF and p_0 is the dimensionless momentum corresponding to the peak of the DF. In this paper we refer to this behaviour of the DF as “short-tailed”. On the other hand, at large opening angles, the DF of the number of particles was found to fall off as $\exp(-p^{0.2})$ at high momenta. In general, [Arendt & Eilek \(2002\)](#) found these latter DF to be significantly broader than those at small opening angles. Therefore, we refer to this type of DFs as “long-tailed”. It must be kept in mind that the simulations by [Arendt & Eilek \(2002\)](#) assume the initial seed photons to be mono-energetic, and relaxing this condition may lead to significant changes in the resulting DFs. Among other pair cascade models, like those by [Hibschman & Arons \(2001\)](#) and by [Suvorov & Chugunov \(1973\)](#) exhibit the presence of a power-law “long-tail” which falls off inversely as the third power of the particle momentum. On the other hand, Monte Carlo models used by [Daugherty & Harding \(1982\)](#) show a “short-tail” in the particle DF (see Fig. 5 of [Hibschman & Arons 2001](#) for comparison). Thus, earlier studies demonstrate the possibility of having both types: short- and long-tailed, DF in pulsar plasma.

For the soliton formation based on the NLSE model (3), we will show below that the presence/absence of an extended tail in the DF is of paramount importance. Namely, it eventually determines the number of plasma particles contributing to the non-linear Landau damping and cubic non-linearity terms in the NLSE. In order to explore this aspect, we choose two representative forms of particle DF, viz., a Gaussian with an exponentially decaying tail (“short-tail”) and a Lorentzian with a power-law tail (“long-tail”).

The particle DF $f_\alpha^{(0)}$ is taken to be a function of the dimensionless momentum p , which is defined as

$$p = \frac{P_\alpha}{m_\alpha c} = \frac{\gamma m_\alpha v}{m_\alpha c} = \gamma \beta \equiv \frac{\beta}{\sqrt{1 - \beta^2}}. \quad (9)$$

where P_α is the relativistic momentum and m_α is the mass of the plasma particles of the α -th species. For the rest of the analysis the term ‘momentum’ would be used to refer to dimensionless momentum of the plasma particles. For both Gaussian and Lorentzian DFs, the term “temperature” will be used to refer to their widths in the momentum space. We will also sometimes refer to the tail of the Lorentzian DF as “high-energy” tail, since particle energy scales approximately as momentum in the ultra-relativistic regime.

As seen from the Table B2 and Table B3 of Appendix B, the integrals in the the dimensionless coefficients G_d, q_d and s_d require the estimation of the group velocity of the particles. For a given DF the wave group velocity (normalized to speed of light c) is estimated from the expression (see Eq. B3 of Appendix B)

$$\beta_{\text{gr}} = \frac{1}{c} \frac{d\omega}{dk} = \frac{1 + \sum_\alpha \left(\frac{\omega_{p,\alpha}}{kc} \right)^2 \int_{-\infty}^{+\infty} dp \frac{\partial f_\alpha^{(0)}}{\partial p} \frac{\beta}{(\beta_{\text{ph}} - \beta)^2}}{\sum_\alpha \left(\frac{\omega_{p,\alpha}}{kc} \right)^2 \int_{-\infty}^{+\infty} dp \frac{\partial f_\alpha^{(0)}}{\partial p} \frac{1}{(\beta_{\text{ph}} - \beta)^2}}. \quad (10)$$

where β_{ph} corresponds to the non-dimensional phase velocity of the linear Langmuir waves (normalized to the speed of light c) and the

dimensional wave number k is given by the expression

$$k = \frac{1}{c} \left[\sum_{\alpha} \omega_{p,\alpha}^2 \int_{-\infty}^{+\infty} dp f_{\alpha}^{(0)} \frac{1}{\gamma^3 (\beta_{ph} - \beta)^2} \right]^{1/2}. \quad (11)$$

where $\omega_{p,\alpha}$ is the plasma frequency associated with α -th species in the plasma and is defined as

$$\omega_{p,\alpha} = \sqrt{\frac{4\pi n_{\alpha} e_{\alpha}^2}{m_{\alpha}}} \quad (12)$$

Note that the dependence of $\omega_{p,\alpha}$ on the particle species comes from its dependence on mass m_{α} , number density n_{α} and the charge e_{α} of the species.

In Section 3 we will also extensively refer to the momentum corresponding to the group velocity, given according to (9), by

$$p_{gr} = \gamma_{gr} \beta_{gr}. \quad (13)$$

This p_{gr} appears as a pole in the integrals for s_d and q_d (see Table B2 and B3 in Appendix B). The location of this pole determines the magnitude of s/q (see Eq. B23 of Appendix B). Physically, $|s/q|$ is higher if the pole p_{gr} is near the peak of the DF since then the number of particles interacting with Langmuir waves is greater, and vice versa.

In the next subsection we discuss under what condition charge separation occurs in the configuration space and how the presence of an iron species component may potentially enhance the charge separation.

2.2 Charge separation in configuration space

The slowly varying charge density (in electrostatic units per cubic centimeters) corresponding to the envelope field of Eq. (3) is given by (see Eq. A23 of MGP00)

$$\rho = \mu \left(\frac{1}{4\pi k^2 c^2} \right) \left(\frac{|e|}{m_e c^2} \right) \frac{\partial^2 |E|^2}{\partial \xi'^2}, \quad (14)$$

where

$$\mu = \frac{\sum_{\alpha} \text{sgn}(\alpha) \varphi_{\alpha} \omega_{p,\alpha}^2 \mathcal{P} \int_{-\infty}^{+\infty} dp \frac{1}{(\beta - \beta_{gr})} \frac{\partial}{\partial p} \left[\frac{(\beta - \beta_{gr})}{(\beta_{ph} - \beta)^2} \frac{\partial f_{\alpha}^{(0)}}{\partial p} \right]}{\sum_{\alpha} \omega_{p,\alpha}^2 \mathcal{P} \int_{-\infty}^{+\infty} p \frac{1}{(\beta - \beta_{gr})} \frac{\partial f_{\alpha}^{(0)}}{\partial p}}, \quad (15)$$

where $\text{sgn}(\alpha)$ is + for positrons and ions, and is - for electrons, and $\varphi_{\alpha} = (|e_{\alpha}|/e) \times (m_e/m_{\alpha})$.

Equation (15) shows that for coinciding electron and positron DF, the terms pertaining to electrons and positrons in the numerator of (14) cancel each other. Then, integral μ vanishes and there is no charge separation. Physically, this effect of charge separation can be understood as follows. The term $\partial^2 |E|^2 / \partial \xi'^2$ represents the ponderomotive/Miller force. The Miller force is a pressure force which pushes plasma particles from regions of strong to low electric fields. The force is independent of the sign of the charge particles but depends on the magnitude of charge to mass ratio of the α -th plasma species. For example, in an electron-ion plasma, the Miller force can push an electron farther away compared to an ion, and hence effective charge separation can be achieved. In the case of pair plasma, since the charge to mass ratio is same for both species, there is no such charge separation possible. Thus, in pulsar relativistic pair plasma for a coinciding electron-positron DF, no charge separation is possible. However, it was pointed out by MPG00 that due to flow of pair plasma along curved magnetic field lines, the electron and positron DF of pair plasma can separate (Cheng & Ruderman 1977; Asseo & Melikidze 1998; Paper I; also see Appendix F for full derivation) and hence relativistic masses of the electrons and positrons can be unequal. Thus, the separation of electron-positron DF can produce an effective charge separation in plasma. As shown in Paper I, the extent of the separation is determined by the arrangement of the non-dipolar surface magnetic field. For various arrangements of that field, the separation of the DF remains nearly constant for around 1000 km above the neutron star surface. In this context, we can treat the separation of the DF as a free parameter, and therefore we will consider several representative values of DF separation in Section 3.

MGP00 also suggested that the presence of an additional heavier iron ion ${}^{56}_{26}\text{Fe}$ with a high magnitude of charge component can enhance the charge separation. The PSG model provides an important motivation for inclusion of an iron ion species as an additional component in the pulsar plasma. One of the goals of the present study is to find out if indeed the presence of an ion species can have appreciable effects on charge separation.

In the next section, we will evaluate the dimensionless coefficients of NLSE expressed in Eq. (4) to Eq. (6) and the charge separation

integral μ from equation (15) as a function of plasma temperature and the separation of the DF. We also include the contribution of a low-density ion component (see Appendix B3).

3 PARAMETER SPACE FOR NLSE FOR SOLITON FORMATION

The NLSE with NLD can be converted into the dimensionless form (see Eq. 20 of LMM18) as

$$i \frac{\partial u}{\partial t} + \frac{\partial^2 u}{\partial x^2} + Qu \left(|u|^2 + \frac{s}{\pi q} \mathcal{P} \int dx' \frac{|u(x', t)|^2}{x - x'} \right) = 0. \quad (16)$$

where

$$u = \frac{E}{E_0}, \quad (17)$$

$$x = \frac{\xi'}{l\theta}, \quad (18)$$

$$t = \frac{\omega_p G_d}{\theta^2} \tau', \quad (19)$$

$$Q = \left[\theta^2 \left(\frac{e}{m_e c^2} \right)^2 \left(\frac{|E_0|^2}{8\omega_p^2 \gamma} \right) \right] \left(2 \frac{q_d}{G_d} \right), \quad (20)$$

where u is the non-dimensional amplitude of the Langmuir wave envelope, x is the non-dimensional space variable, t is the non-dimensional time variable, Q represents the non-dimensional ratio of the cubic non-linearity coefficient q to the group velocity dispersion. Here, the characteristic length l of the linear Langmuir waves is given by

$$l = \frac{2\pi}{k}, \quad (21)$$

where k is the wave number as defined in Eq. (11). The quantity $\theta/2\pi$ is a spatial scaling variable which characterizes the ratio of the spatial extent of the nonlinear wave envelope to the characteristic length l of linear Langmuir waves. Similarly to LMM18, we will use a value $\theta = 100$ in the estimates of typical soliton properties, which will be presented in subsection 3.1. For simplicity, the term in the square brackets in Eq. (20) for Q will be taken to equal 1, given that E_0 is an unknown field amplitude. The quantity $Q = 2q_d/G_d$ has to be positive to fulfill the Lighthill condition (2). Physically, the typical soliton formation timescales are on the order of $\sim O(1/Q)$. Thus, soliton formation is delayed for smaller Q and vice versa.

Solving Eq. (16) requires us to specify an initial condition. LMM18 represented the initial condition as a combination of the constant electric field component and a random electric field component. For our analysis, we discount any constant electric field and use only a completely disordered electric field (LMM18):

$$u(x, 0) = \int_{-\infty}^{+\infty} dk \frac{\hat{w}(k) \exp[-0.5(k/k_{\text{corr}})^2 - ikx]}{\sqrt{\sqrt{\pi} k_{\text{corr}}}}. \quad (22)$$

Here k_{corr} is the wave number corresponding to the correlation length l_{corr} such that

$$k_{\text{corr}} = \frac{2\pi}{l_{\text{corr}}}, \quad (23)$$

and quantity $\hat{w}(k)$ denotes a white noise field described by

$$\langle \hat{w}(k_1) \hat{w}(k_2) \rangle = 0, \quad (24)$$

$$\langle \hat{w}^*(k_1) \hat{w}(k_2) \rangle = 2\delta(k_1 - k_2), \quad (25)$$

where the angle brackets denote ensemble average. Let us mention that increasing k_{corr} has the same effect as decreasing Q : they both increase the time at which solitons emerge; see Table 2 of LMM18.

To solve Eq. (16) numerically, we use the Integrating Factor-Leap-frog method by Lakoba (2017). Simulation parameters of the numerical scheme are summarized in Appendix C.

Next, the maximum dimensionless time for soliton formation can be estimated as follows. The derivation of Eq. (16) assumes that background plasma conditions as captured by the coefficients (4)-(6) are steady during the evolution of the wave electric field. For any given separation of the DF, this condition requires that the plasma frequency ω_p should not change drastically during the evolution of the wave electric field. From Eq. (8), the change in plasma frequency $\Delta\omega_p$ for segments of Δr km along a field line can be estimated to be $\Delta\omega_p/\omega_p = 1.5\Delta r/r$. Thus, if we choose $\Delta r = 3$ km and $r = 500$ km, the change in plasma frequency is less than 1% and can indeed be neglected. Since the outflow is ultra-relativistic, a typical timescale associated with this spatial length segment is $\Delta t_{\text{OFR}} = 3 \text{ km}/c \approx 10^{-5}$ seconds. We assume that the PFR moves with a Lorentz factor $\gamma_s \approx 200$ with respect to OFR. Then, the typical timescale in the PFR is $\Delta t_{\text{PFR}} = \gamma_s \Delta t_{\text{OFR}} \approx 2 \times 10^{-3}$ seconds. The MFR moves relative to OFR in the same direction as PFR (away from the pulsar along the

magnetic field lines) with a typical Lorentz factor $\gamma_{\text{gr}} \approx p_{\text{gr}}$ (see (13)) with respect to PFR. Combining Lorentz factors for ultra-relativistic co-propagation (see Appendix G), we find that the maximum timescale in MFR is:

$$\tau'_{\text{max}} \approx 2p_{\text{gr}} \Delta t_{\text{PFR}}. \quad (26)$$

Next, at a typical distance of 500 km from the surface we find, using Eq. (19), that the maximum dimensionless time t_{max} is given by

$$t_{\text{max}} \approx 10^4 \left(\frac{\omega_p}{10^8 \text{ rad s}^{-1}} \right) \left(\frac{100}{\theta} \right)^2 G_d \tau'_{\text{max}}, \quad (27)$$

where we have used that for the typical parameters assumed in this study, $\omega_p \sim 10^8 \text{ rad s}^{-1}$; see Eq. (8). In subsection 3.1 we will see that in those cases when solitons are formed, one can take $p_{\text{gr}} \approx 6$ and $G_d \lesssim 10$ as representative values. Then Eq. (26) yields $\tau'_{\text{max}} \approx 2 \times 10^{-2}$ seconds and Eq. (27) yields the following estimate for the maximum dimensionless time t_{max} where the (3) can be applicable:

$$t_{\text{max}} \sim 2 \times 10^3 \left(\frac{\omega_p}{10^8 \text{ rad s}^{-1}} \right) \left(\frac{100}{\theta} \right)^2 \left(\frac{G_d}{10} \right) \left(\frac{\tau'_{\text{max}}}{2 \times 10^{-2} \text{ sec}} \right). \quad (28)$$

Thus, for the Lorentzian DF, the maximum dimensionless time of the simulation can be restricted to about 2000 units.

In fact, we observed solitons form over dimensionless times that are some two orders of magnitude smaller than the above estimate. This indicates that either solitons can form over distances much less than the above estimate of $\Delta r = 3 \text{ km}$, or that the factor in the square brackets in (20), which we had assumed to equal 1, can in fact be much smaller (thereby allowing a larger range of values for the dimensional field intensity $|E_0|^2$, or a combination of both. In other words, a large range of values for the intensity of the initial linear field will be able to lead to soliton formation as long as the condition on $|s/q|$ stated in the next subsection is fulfilled.

3.1 Lorentzian DF

Let us use the Lorentzian DF to get representative values of the ratios s/q , q_d/G_d and the dimensionless group velocity dispersion G_d . After obtaining these representative values, we will explore soliton formation numerically following the method of Lakoba (2017) and LMM18.

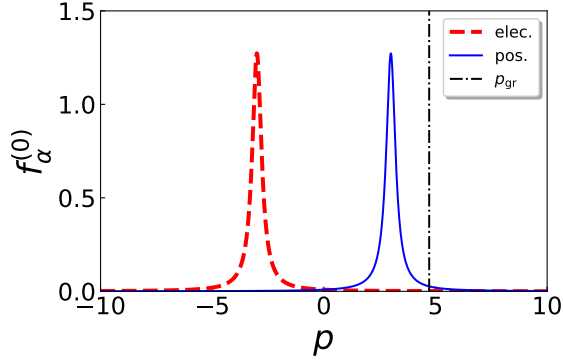
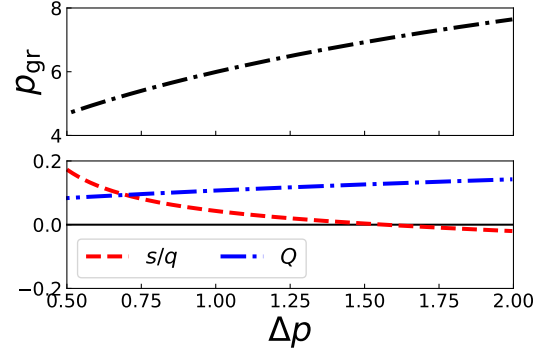
The Lorentzian DF for the α -th species is given by

$$f_{\alpha}^{(0)} = \frac{1}{\pi} \frac{\frac{1}{2} \Delta p}{(p - p_{\alpha})^2 + \left(\frac{1}{2} \Delta p \right)^2}, \quad (29)$$

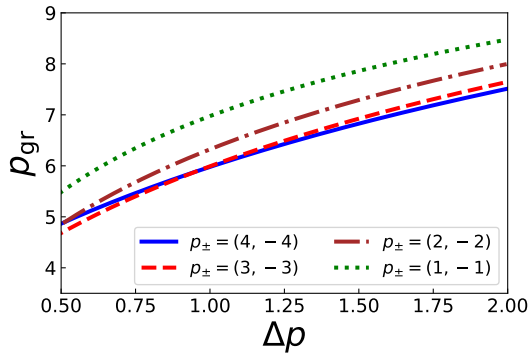
where Δp is the width of the DF and p_{α} is the peak of the DF. Here $\alpha = \pm$ refers to the positron and the electron DF, respectively. In this subsection we refer to Δp of Eq. (29), which characterizes the spread of particles' momenta, as ‘‘temperature’’. In relativistic hot plasma, this spread of the momenta is assumed to be a significant fraction of the mean momentum. Contrarily, in a cold plasma, the spread is small. Next, in this study we assume the peak momentum of the particle DF to vary in the range 1 to 3. Thus, to keep the ratio of the width to the peak in the DF to vary from the cold limit to hot limit at all values of peak separation, $p_+ - p_-$, the plasma temperature Δp is chosen to be in the range (0.5, 2.0) in this study. In dimensional units, this temperature range corresponds to $5 \times 10^9 \text{ K}$ to $2 \times 10^{10} \text{ K}$.

We evaluate the NLSE coefficients at different separations of the DF as a function of the plasma temperature using Eqs. B6, B9 and B12 of Appendix B. The results are shown in Fig. 1 and can be understood physically as follows. Panel (A) shows for a given separation of the DFs, the pole due to group velocity p_{gr} is at the tail of DF. The upper sub-panel of Panel (B) shows that the pole p_{gr} shifts to higher values as the temperature of the plasma is increased. Thus, the number of interacting particles at the group velocity decreases as the temperature is increased. It is reflected in the lower sub-panel of Panel (B), which shows that the magnitude of s/q decreases with increasing plasma temperature. Next, we explore the location of the pole due to group velocity p_{gr} for different separation of DF. Panel (C) shows that at a given plasma temperature (say $\Delta p = 1.0$) the pole p_{gr} shifts to lower values as the separation of the DFs increases. It means that with increasing separation of DF, the pole shifts towards the center of the DF, thereby increasing the number of plasma particles interacting with the Langmuir waves, thereby increasing the effect of the nonlinear Landau damping relative to the instantaneous cubic nonlinearity. Consequently, panel (D) shows that for moderate separation values, the magnitude of s/q is clustered within ~ 0.1 from zero for a range of plasma temperatures. However, for larger separation of DF, the magnitude of s/q increases to about 0.5 or even higher, especially for colder plasma. Finally, panel (E) shows that the quantity Q is on the order of ~ 0.25 for all separations of the DF across the range of plasma temperatures. Thus, we take $s/q = 0.1$ and 0.5 for small/moderate and for larger DF separation, respectively. The value of Q can be taken to have a constant value of 0.25.

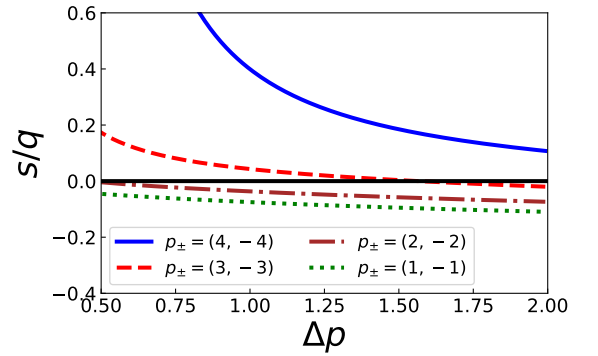
Simulation results for ($Q = 0.25$, $s/q = 0.1$) and the initial condition (22) are shown in Fig. 2. Following LMM18, we used a representative value $k_{\text{corr}} = 2$. In Panel (A) soliton formation can be clearly identified with the movement of a well-formed secondary spectral peak from $k = 0$ to $k < 0$. This peak in the Fourier spectrum corresponds to a soliton in physical space (LMM18), seen in Panel (B). Panel (C) shows the Miller force associated with the envelope soliton.

(A) Lorentzian DF and group velocity pole with $p_{\pm} = \pm 3$ at $\Delta p = 0.5$.

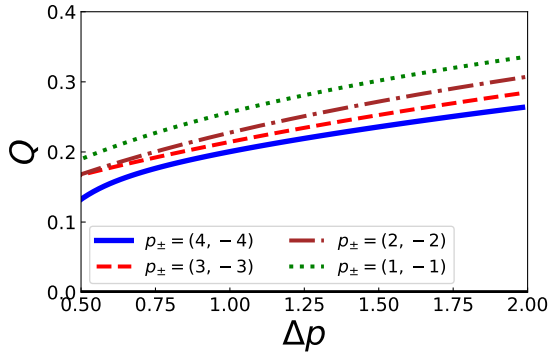
(B) Parameter space for Panel (A) as a function of temperature.



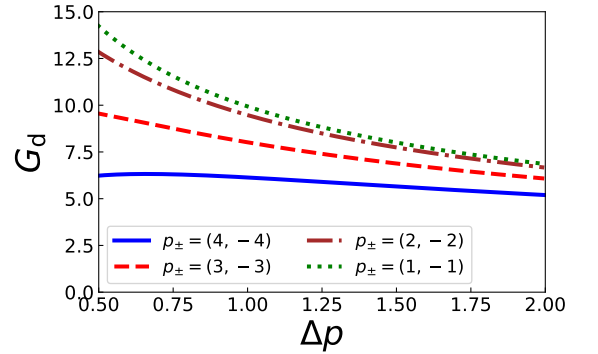
(C) The group velocity pole as a function of temperature and separation of DF.



(D) Ratio of NLD to CNL as a function of temperature and separation of DF.



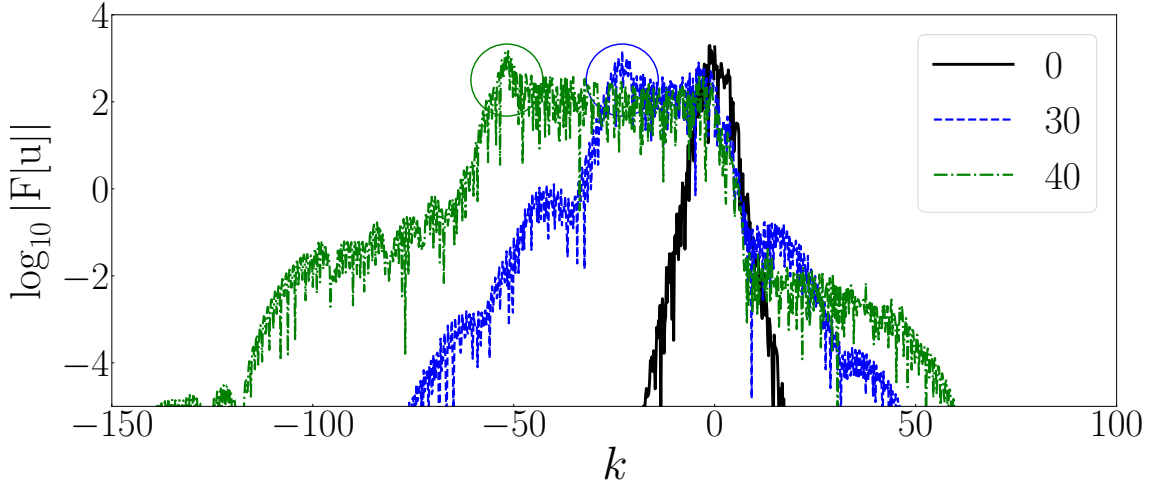
(E) The Lighthill condition as a function of temperature and separation of DF.



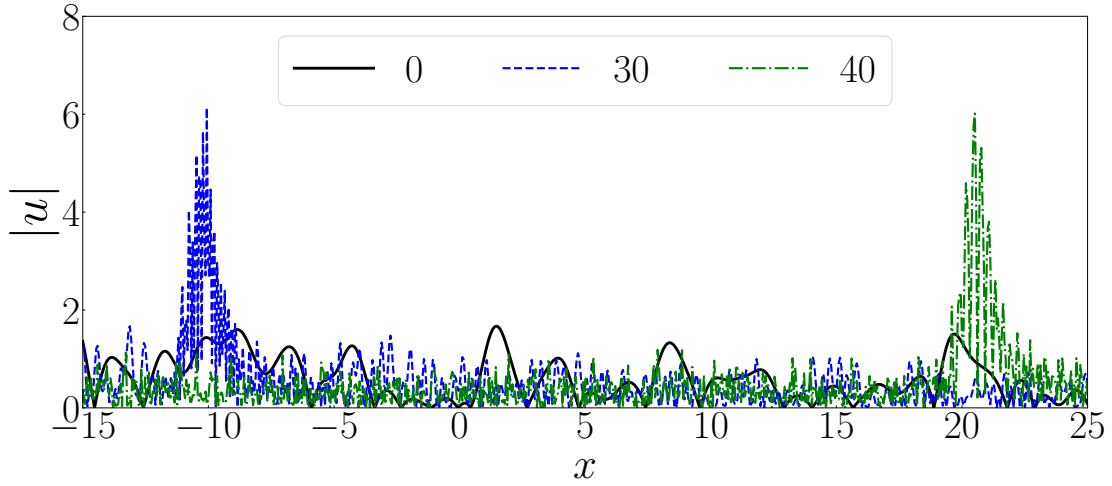
(F) GVD as a function of temperature and separation of DF.

Figure 1. The figure shows temperature dependence of NLSE coefficients for separated Lorentzian DF as defined in equation (29). **Top:** Panel (A) shows a particular example of separated electron and positron DF along with the group velocity pole p_{gr} as defined in Eq. (13) for a particular temperature. Panel (B) shows the variation of p_{gr} , s/q and q_d/G_d as a function of temperature at the same separation of DF as shown in Panel (A). **Middle:** Panel (C) shows that p_{gr} at a given plasma temperature decreases as the separation of the DF increases. Panel (D) shows that the ratio s/q remains tightly clustered to values within 0.1 of zero for moderate separation of DF. Only at sufficiently high separation of DF can the s/q ratio increase to values higher than 0.5. **Lower:** Panel (E) shows that Q stays within the range (0.1, 0.3) for the range of plasma temperatures considered; in particular, the Lighthill condition (2) is satisfied. Panel (F) shows that the group velocity dispersion at any temperature decreases with increasing separation.

The following remark about identifying soliton formation from the field's spectrum needs to be made. In panel (A) one sees that the amplitudes of the secondary peak, corresponding to the soliton in the physical space, and of the spectrum of the initial field are about the same. Yet, the amplitude of the soliton in the physical space (panel (B)) is several times greater than that of the initial field. Thus, this amplitude increase must occur via increased coherence of the field “inside” the secondary spectral peak compared to the initial fully random field. As was noted in LMM18, this formation of high-amplitude solitons out of an initial disordered state is a generic feature that occurs in many



(A) Electric field evolution in the Fourier space



(B) Electric field evolution in the configuration space (for a selected range).

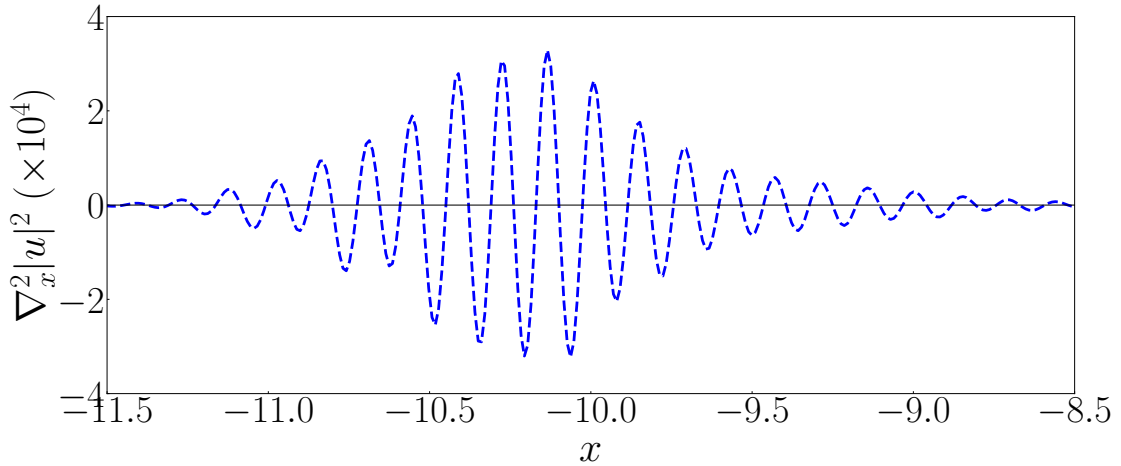
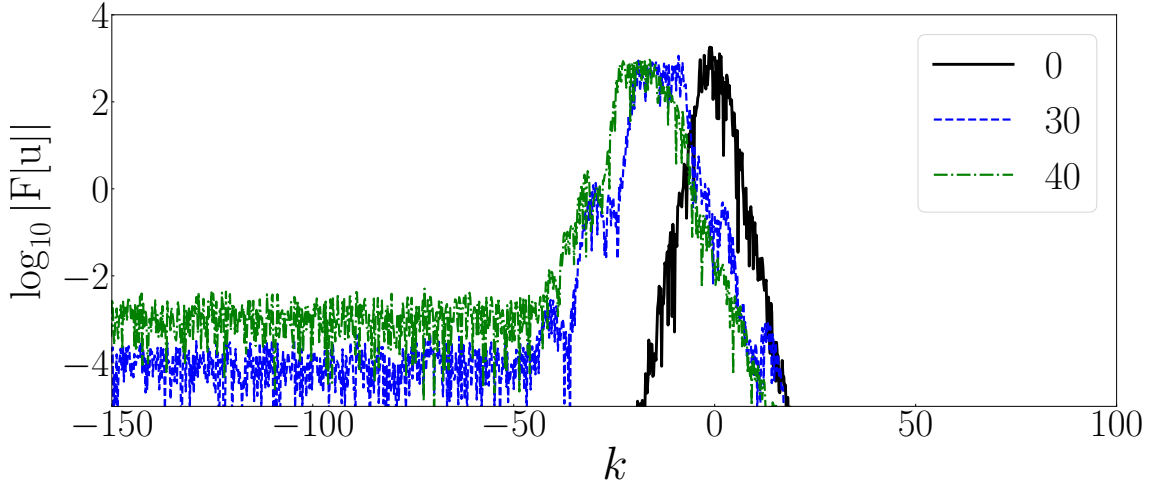
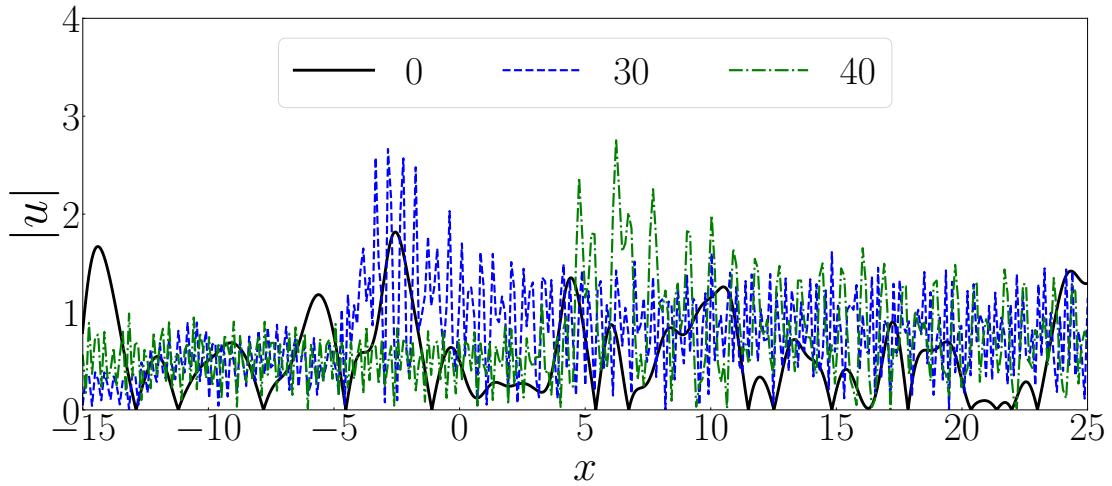
(C) The Miller force associated with soliton electric field at $t = 30$.

Figure 2. Simulation results of soliton formation for Lorentzian DF ($Q = 0.25$ and $s/q = 0.1$) by the numerical method described in Lakoba (2017). Panel (A) shows the movement of a prominent secondary peak (circled) to $k < 0$ at few representative times. Panel (B) shows the corresponding soliton formation in configuration space in the limited range $(-15, 25)$ for clarity. The actual simulation box has the range $(-60, 60)$. The legends in both panels indicate the dimensionless time t . The black curve in both panels shows the initial condition at $t = 0$. Panel (C) shows the Miller force associated with the soliton electric field at $t = 30$. Here ‘soliton’ is the envelope of the pulse with $\Delta x \sim 3$ units while ripple is what appears to be a “carrier wave” with wavelength $\delta x_{\text{ripple}} \sim 0.15$ units.



(A) Electric field evolution in the Fourier space.



(B) Electric field evolution in the configuration space (for a selected range).

Figure 3. Simulation of pulse evolution for Lorentzian DF ($Q = 0.25$ and $s/q = 0.5$) by the numerical method described in Lakoba (2017). The black curve in both panels shows the initial condition at $t = 0$. Panel (A) shows the absence of a prominent secondary peak as was seen in Fig. 2. Panel (B) shows the corresponding wave field evolution in the configuration space in the limited range $(-15, 25)$ for clarity. The actual spatial range of the simulation box is $(-60, 60)$. It can be seen that the amplitude of the envelope of the pulses at any time does not exceed the amplitude of the initial wave electric field. Thus, soliton formation is suppressed for $s/q \geq 0.5$.

(but not all) so-called “near-integrable but not exactly integrable” nonlinear wave models. (Here, the case $s/q = 0$ is that of the integrable NLSE with purely local cubic nonlinear term; for it, formation of a long-living soliton out of a disordered state will *not* occur.) The specific contributions of this study, and earlier of LMM18, was to show that this soliton formation does indeed occur for the NLSE with a sufficiently small nonlinear Landau damping term, *and* that it occurs within the time t_{\max} that corresponds to realistic parameters in pulsar plasma. (In contrast, soliton formation in another model, considered in Jordan & Josserand (2001), occurred over a time of many tens of thousands dimensionless units.)

The simulation results for ($Q = 0.25$, $s/q = 0.5$) are shown in Fig. 3. Unlike in Fig. 2, here no spectral peak is seen to form in Panel (A), and, instead, energy gets more uniformly distributed among spectral components of the field. One can interpret this as the field becoming less coherent for those larger values of s/q . In physical space (Panel (B)), this is manifested by the absence of well-localized, long-living and high-amplitude bunches of electric field. It must be noted that the behaviours, shown in Figs. 2 and 3, at small and large s/q were found in LMM18, whereas here we demonstrated that they can actually occur in pulsar plasma.

Next, since our assumptions at the beginning of this section about the strength of the electric field (i.e., parameter Q) and the measure of disorder of the initial field (i.e., k_{corr} in (22)) are somewhat arbitrary, below we explore the effect of these parameters on soliton formation. The simulation setup and technical details of the results are described in Appendix D; here we present only their gist. First, we found that the effect of decreasing k_{corr} from 2 to 1 led only to the decrease of the soliton formation time, in accordance with the statement at the beginning of this Section; no statistically significant changes were found in the distribution of the amplitude of the long-living solitons that formed.

Second, we doubled the initial amplitude of $u(x, 0)$, which is tantamount to quadrupling Q . In this case, the final amplitude of the formed solitons was, on average, lower than for the original $u(x, 0)$; however, qualitatively, the distribution of the final soliton amplitudes remained similar to the original case. (We also found that, in agreement to the statement at the beginning of this Section, the soliton formation time decreased approximately four-fold.)

To summarize, soliton formation for long-tailed DF can occur for a wide range of plasma temperature for moderate separations of the electron-positron DF. Large separation of the DF increases the value of s/q , which necessarily leads to suppression of soliton formation via the mechanism explained in our discussion about Fig. 1

3.2 Gaussian DF

The Gaussian DF for α -th species is given by

$$f_{\alpha}^{(0)} = \frac{1}{\sqrt{2\pi}\sigma} \exp\left\{-\frac{(p - p_{\alpha})^2}{2\sigma^2}\right\}, \quad (30)$$

where σ is the width of the DF and p_{α} is the peak of the DF. In this subsection, we will refer to σ as the plasma “temperature”. Like in the previous subsection, in our study the plasma temperature σ is restricted to the range (0.5, 2.0).

Similar to the previous subsection, we evaluate the NLSE coefficients for different separations of the Gaussian DF as a function of the plasma temperature σ . The results are shown in Fig. 4 and can be understood physically as follows. Panel (A) shows that for a given separation of the DF, the pole due to group velocity p_{gr} is near the center of the positron DF. The upper sub-panel of Panel (B) shows that while pole p_{gr} shifts to higher values with increasing temperature, it still lies very close to the peak of the positron DF. Thus, the number of particles that can interact at the group velocity of linear Langmuir waves remains high. This is reflected in the lower sub-panel of Panel (B), which shows that the magnitude of s/q generally remains high across a range of σ . Next, we explore the location of p_{gr} for different separations of DF. Panel (C) shows that for all temperature values considered, the pole p_{gr} remains close to the center of the positron DF. Panel (D) shows that small values of s/q can be obtained only in a very narrow range of σ where the quantity s/q changes sign. The location of this temperature range varies with the DF separation and, in fact, for sufficiently small separation, there is no temperature (in the range considered here) where s/q would be as small as 0.1. Namely, for $p_{\pm} \sim \pm 1$, one has $s/q \sim -0.5$.

As shown in Fig. 3 and in LMM18, higher values of $s/q \gtrsim 0.5$, observed for most temperature values in the above range, lead to suppression of soliton formation.

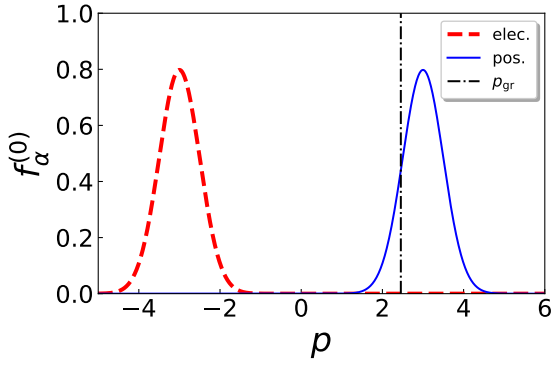
To summarize, the Gaussian DF provides small values of $s/q \lesssim 0.1$ only in a narrow interval of temperatures and for moderate separation of DF. As the DF separation decreases, the interval where s/q remains small, shrinks and eventually vanishes, and the ratio stays too high: $s/q \approx -0.5$, for solitons to form. This leads us to conclude that soliton formation for short-tailed DF can occur only in a very restrictive parameter regime. As a result, short-tailed DF seems to be unlikely candidates for sustaining soliton formation under generic hot plasma conditions.

3.3 Dependence of soliton formation on sign of s/q

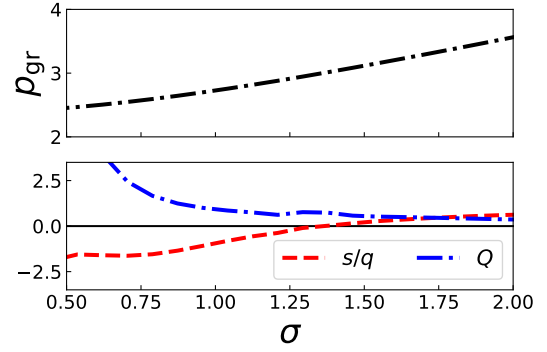
It can be seen from Panel (D) of Fig. 1 and Fig. 4 that the ratio s/q can be both positive and negative. Physically, the sign of s/q only determines the direction of the movement of the secondary peak associated with soliton formation to a higher wave number in the Fourier space (LMM18). For negative s/q , the secondary peak in the Fourier space moves to $k > 0$ and vice versa. Physically, there is no difference as the presence of a secondary peak for both $k > 0$ and $k < 0$ gives rise to envelope solitons in the configuration space. The soliton formation timescale is not affected in a statistical sense. To show that this is indeed the case, we simulate soliton formation for $Q = 0.25$ for $s/q = 0.1$ and $s/q = -0.1$ for 200 random seed values for the white noise in Eq. (25). Figure 5 shows the histogram for the time t of soliton formation, defined as

$$\max|u(x, t > 0)| \geq 3 \times \max|u(x, 0)|. \quad (31)$$

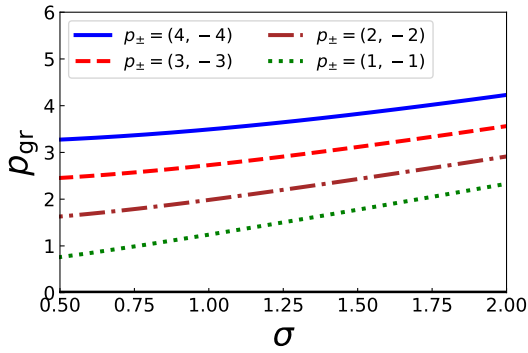
It can be seen that the statistics of soliton formation times indeed does not depend on the sign of s/q .

(A) Gaussian DF and group velocity pole with $p_{\pm} = \pm 3$ at $\sigma = 0.5$.

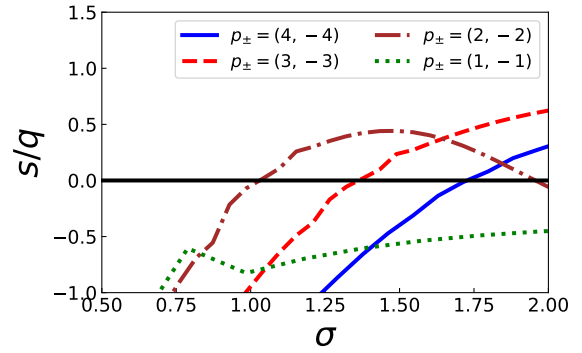
[h]



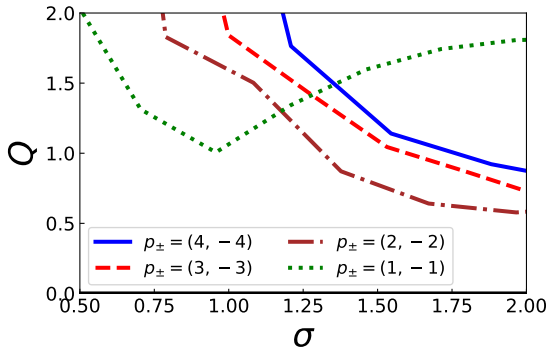
(B) Parameter space for Panel (A) as a function of temperature.



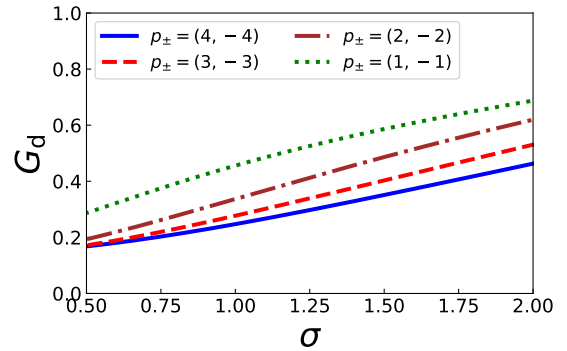
(C) The group velocity pole with temperature and DF separation.



(D) Ratio of NLD to CNL as a function of temperature and separation of DF.



(E) Lighthill condition as a function of temperature and separation of DF.



(F) GVD as a function of temperature and separation of DF.

Figure 4. The figure shows temperature dependence of NLSE coefficients for separated Gaussian DF as defined in equation (30). **Top:** Panel (A) shows a particular example of separated electron and positron DF along with the location of the group velocity at the same temperature. Panel (B) shows the variation of p_{gr} , s/q and Q as a function of temperature at the same separation of DF as shown in Panel (A). **Middle:** Panel (C) shows that the p_{gr} for a given plasma temperature increases as the separation of the DF increases. Panel (D) shows that the ratio s/q remains large for all separation of DF. The moderate values of s/q are available only near a certain temperature σ_{sp} where s/q changes sign. The value of σ_{sp} decreases with decreasing separation of the DF, until below some separation it vanishes and the magnitude of s/q ratio settles at around 0.5. **Lower:** Panel (E) shows that the Lighthill condition (2) is satisfied across the range of plasma temperatures. Panel (F) shows that the group velocity dispersion remains clustered around 0.4 for all separation of DF across a wide range of plasma temperatures.

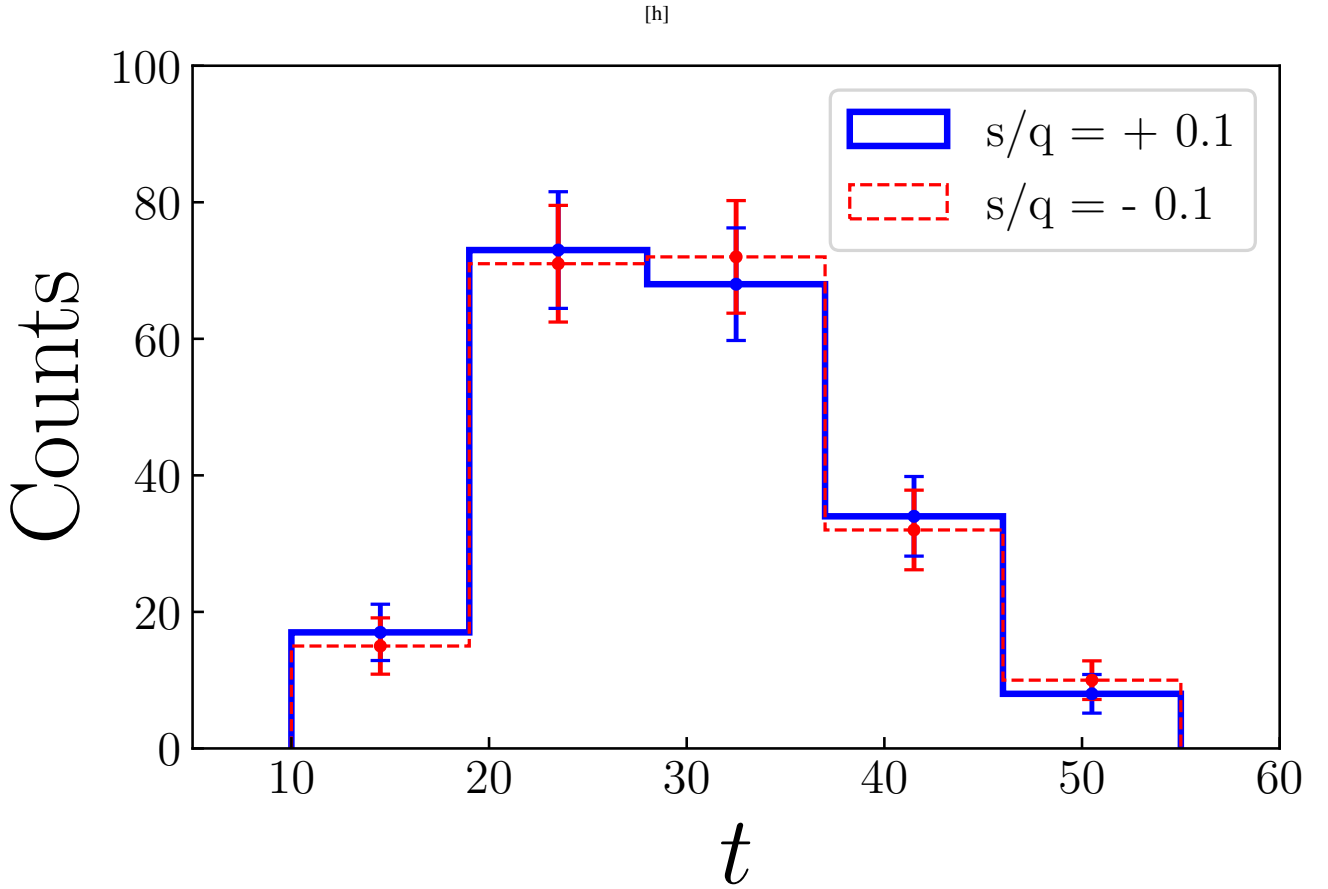


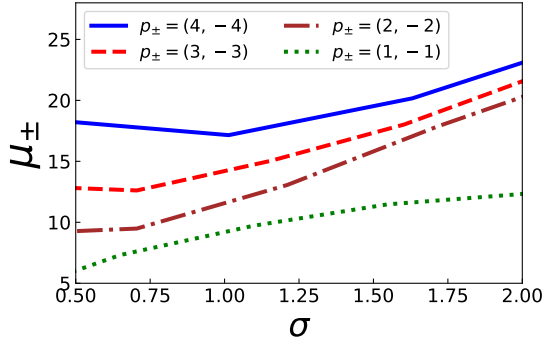
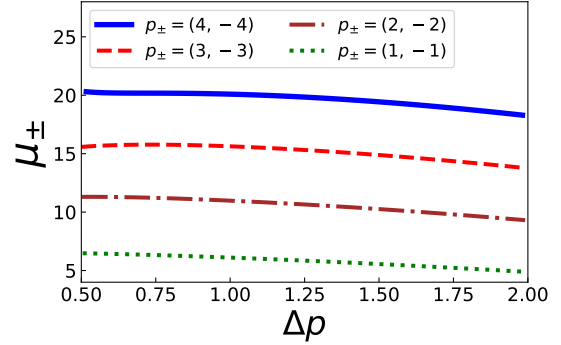
Figure 5. The figure shows the histogram for the earliest soliton formation time t (with $Q = 0.25$) which satisfies the constraint (31) for 200 random seeds in equation (25) for both positive $s/q = +0.1$ (shown in solid blue) and negative $s/q = -0.1$ (shown in dashed red). The histogram for t is divided into 5 bins in the range (10, 55) while the error bars $= \sqrt{N}$ where N is the number of entries in each bin. It can be seen that the the average time for soliton formation is ~ 30 units for both signs of s/q .

3.4 Role of ions in modifying the coefficients of NLSE

The DF of ions are expected to be near the electron and positron DF. We treat the location of the ion DF as a free parameter wherein the maximum contribution to the NLSE coefficients due to ions can only come if the center of ion DF is near the pole p_{gr} . The setup for maximizing the contribution to NLSE coefficients due to ions is described in Appendix B4. We find that the presence of ions modify the dimensionless coefficients of NLSE (i.e., G_d, q_d, s_d) by less than 10^{-8} . The result can be understood qualitatively as follows. It must be noted in the PSG model (Gil et al. 2003) the number density of ions is close to 90% of the Goldreich-Julian co-rotational number density. As defined in the Introduction, κ is the ratio of the number density of the pair plasma to the Goldreich-Julian number density. Thus, for simplicity, the ratio of the number density of pair plasma to the number density of ions can be assumed to be κ . Then, the number density of the ions is $\sim 10^4$ times smaller than that of the pair plasma while the mass of the ions is $\sim 10^4$ times higher than that of electrons and positrons. A combination of these two effects reduces the contribution of ions to the coefficients of NLSE by the factor 10^{-8} . A more expanded discussion of these aspects will be presented in the following section. We conclude that ions make negligible contribution in modifying the coefficients of NLSE.

4 TYPICAL PROPERTIES ASSOCIATED WITH LANGMUIR SOLITONS

The typical properties of Langmuir solitons such as spatial extent, structure and charge are crucial in determining if these solitons can be a suitable candidate for the observed coherent radio emission in pulsars. In this section we briefly discuss these aspects.

(A) Contribution to μ from separated electron-positron Gaussian DF.(B) Contribution to μ from separated electron-positron Lorentzian DF.

[h]

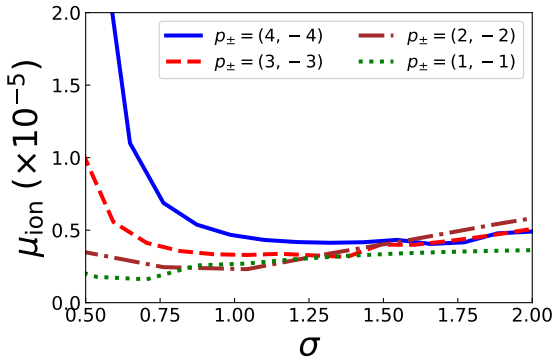
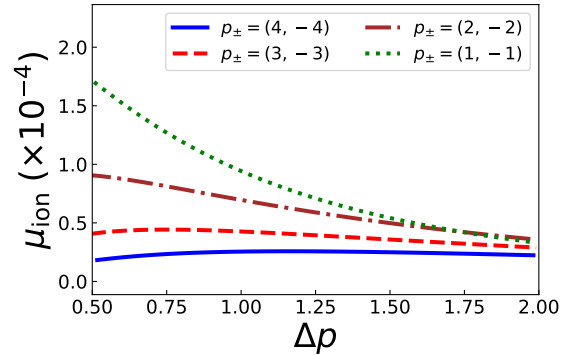
(C) Contribution to μ for Gaussian ion DF.(D) Contribution to μ for Lorentzian ion DF.

Figure 6. Variation of the charge separation integral μ as defined in Eq. (15) for different separation of the DF. Panel (A) and Panel (B) shows that the integral as a function of the plasma temperature for Gaussian and Lorentzian DF respectively. Panel (C) and Panel (D) shows the contribution to the integral due to the presence of an iron ion component. Note the vertical axis scale in Panels (C) and (D) are 10^{-5} and 10^{-4} , respectively.

4.1 Typical length and ripple associated with the solitons

In this subsection, following LMM18 we estimate the typical size of the soliton and the ripple associated with it (in dimensional units) at a distance of $r = 500$ km above the neutron star surface. Using Eq. (11) and Eq. (8), the typical Langmuir length scale l in PFR is given by

$$l = \frac{2\pi}{k} = \frac{\pi c}{\omega_p \sqrt{\gamma}} \approx 6 \times 10^2 \left(\frac{3}{\gamma}\right)^{1/2} \text{ cm.} \quad (32)$$

where $\gamma = \int dp \sqrt{1 + p^2} f_\alpha^{(0)}$ is the average Lorentz factor of the electron/positron DF of the pair plasma in PFR and depends on the temperature of the particles. For the cold plasma limit, γ equals the Lorentz factor at the peak of the electron/positron DF, whereas for hot plasma, γ can be as much as twice the Lorentz factor evaluated at DF's peak. For the rest of the analysis, we choose a representative value of γ to be 3.

From panel (C) of Fig. (2), the typical size of the soliton envelope Δ_{PFR} in PFR is given as

$$\begin{aligned} \Delta_{\text{PFR}} &= \frac{\Delta \xi'}{\gamma_{\text{gr}}} = \frac{l \theta \Delta x}{\gamma_{\text{gr}}} \\ &\approx 3 \times 10^4 \left(\frac{6}{\gamma_{\text{gr}}}\right) \left(\frac{\theta}{100}\right) \left(\frac{\Delta x}{3}\right) \left(\frac{3}{\gamma}\right)^{1/2} \text{ cm,} \end{aligned} \quad (33)$$

while the typical ripple size $\Delta_{\text{ripple,PFR}}$ from panel (C) of Fig. 2 associated with the soliton in PFR is given as

$$\begin{aligned} \Delta_{\text{ripple,PFR}} &= \frac{l \theta \delta x_{\text{ripple}}}{\gamma_{\text{gr}}} \\ &\approx 10^3 \left(\frac{6}{\gamma_{\text{gr}}}\right) \left(\frac{\theta}{200}\right) \left(\frac{\delta x_{\text{ripple}}}{0.15}\right) \left(\frac{3}{\gamma}\right)^{1/2} \text{ cm.} \end{aligned} \quad (34)$$

Then, in OFR, the typical soliton size is

$$\begin{aligned} \Delta_{\text{OFR}} &= \frac{\Delta_{\text{PFR}}}{\gamma_s} \\ &\approx 10^2 \left(\frac{6}{\gamma_{\text{gr}}} \right) \left(\frac{\theta}{100} \right) \left(\frac{\Delta x}{3} \right) \left(\frac{3}{\gamma} \right)^{1/2} \left(\frac{200}{\gamma_s} \right) \text{ cm}, \end{aligned} \quad (35)$$

while the ripple size is

$$\begin{aligned} \Delta_{\text{ripple, OFR}} &= \frac{\Delta_{\text{ripple, PFR}}}{\gamma_s} \\ &\approx 5 \left(\frac{6}{\gamma_{\text{gr}}} \right) \left(\frac{\theta}{100} \right) \left(\frac{\delta x_{\text{ripple}}}{0.15} \right) \left(\frac{3}{\gamma} \right)^{1/2} \left(\frac{200}{\gamma_s} \right) \text{ cm}. \end{aligned} \quad (36)$$

For the case considered in subsection 3.1 where solitons could form (i.e., $s/q = 0.1$) and for representative parameters values considered there, the typical size for the envelope and the ripple associated with solitons are about 100 cm and 5 cm, respectively.

These spatial scales correspond to a frequency range from 300 MHz to 6 GHz, which spans the observed broad-band frequencies of curvature radiation. For a typical radius of curvature $r_c \approx 10^8$ cm in the radio emission zone, the characteristic frequency of curvature radiation is $\nu_c \approx 3\gamma_s^3 c / 4\pi r_c \approx 2$ GHz, which indeed falls into the above range (0.3, 6) GHz. However, the calculation of an actual radiation pattern due to coherent curvature radiation by an *ensemble* of such rippled structures, as can be expected in pulsar plasma, is beyond the scope of this work and will be studied elsewhere.

It must also be noted that the temperature dependence of the size of the solitons is due to the average Lorentz factor γ of the plasma particles and the Lorentz factor corresponding to the group velocity of the plasma waves γ_{gr} . As mentioned earlier, γ for a high-temperature plasma can be twice as large as the Lorentz factor associated with the peak of the electron/positron DF and enters as a square root dependence in the size estimates (35) and (36). As seen from Panel (C) of Fig. 1 and 4, the group velocity changes only marginally within the range of temperature considered. Thus, an increase in temperature can decrease the estimates of the soliton size and ripple size by at most $\sim 30\%$.

It must also be mentioned that the number of ripples within the soliton can vary significantly. Figure 5 shows that, for ($Q = 0.25$, $s/q = 0.1$, $k_{\text{corr}} = 2$), the time of soliton formation (see (31)) has a significant spread and depends on the particular realization of the random initial condition (22). As a result, location (in Fourier space) of the secondary spectral peak has a wide variation. In Appendix E, we show representative cases of the location of the peak in Fourier space and the Miller force associated with the solitons. We find that while the size of the solitons is roughly the same, the number of ripples within the soliton depends on the location of the secondary peak. In particular, the number of ripples increases as the secondary peak shifts towards higher k values. The impact of the variation of the ripple size on radiation pattern will be studied in an upcoming work.

4.2 Charge separation associated with Langmuir solitons

The slowly-varying charge density (14) can be re-written using Eq. (17), Eq. (18) and Eq. (21) as

$$\rho = \mu \left(\frac{e}{m_e c^2} \right) \frac{|E_o|^2}{4\pi k^2 c^2} \frac{1}{l^2 \theta^2} \frac{\partial |u|^2}{\partial x^2}, \quad (37)$$

where the field amplitude $|E_o|^2$ can be expressed in the form

$$|E_o|^2 = \varkappa 8\pi \rho_{\text{GJ}} \kappa c^2 \gamma, \quad (38)$$

where ρ_{GJ} is the co-rotational Goldreich-Julian charge density in OFR, κ is the ratio of the number density of the pair plasma to the co-rotational Goldreich-Julian number density, $\gamma \approx p_+$ is the average Lorentz factor of the plasma particles in PFR and \varkappa is the ratio of the energy density associated with the envelope field and the particle energy density in PFR.

Using the same representative values as above and a typical value $\varkappa \sim 0.1$ (from MGP00), Eq. (37) and Eq. (38) can be combined to give:

$$\frac{\rho}{\rho_{\text{GJ}}} \approx \mu \left[\left(\frac{\varkappa}{0.1} \right) \left(\frac{\gamma}{3} \right) \left(\frac{\kappa}{10^4} \right) \left(\frac{100}{\theta} \right)^2 \left(\frac{1}{4 \times 10^4} \frac{\partial |u|^2}{\partial x^2} \right) \right], \quad (39)$$

where the quantity μ defined in Eq. (15) can be expressed in the form

$$\mu = \mu_{\pm} + \mu_{\text{ion}}, \quad (40)$$

where μ_{\pm} is the contribution due to separation of electron-positron DF and μ_{ion} is the contribution due to iron ion DF near the pole p_{gr} (see Appendices B3 and B4). The variation of μ with temperature is shown in Fig. 6. It can be seen that separation of electron and positron DF

leads to $\mu_{\pm} \sim 10$. It can also be seen that ions play negligible role in charge separation since the highest value of $\mu_{\text{ion}} \approx 10^{-4}$. The result can be understood physically as follows. The response of α -th species to the Miller force ($\nabla^2|E|^2$) depends on the mass and density of the species. We find that the very small number density of the ions and their heavier mass leads to this response being weak. On the other hand, the separation of electron and positron DF in the pair plasma changes the effective relativistic mass (“inertia”) of the electrons and positrons. Thus, the Miller force acts differently on both species to create a spatial charge separation. Panels (A) shows that μ_{\pm} for Gaussian DF varies with temperature while Panel (B) shows that for Lorentzian DF, μ_{\pm} remains steady across a wide range of plasma temperatures. This implies that for the same separation of the DF, the effective mass is temperature-dependent for short-tailed DF and is nearly temperature independent for long-tailed DF. For ions, the nature of the DF determines the number of interacting particles at p_{gr} . For ions with large mass $m_{\text{ion}} = Am_p$, where m_p is the mass of the proton and A is the atomic weight, the choice of DF has negligible effect on the change in ions’ relativistic mass.

Let us now demonstrate that there is no physically feasible solution where contribution of ions to the charge density separation could be non-negligible (i.e., comparable to that contribution from electrons and positrons). The expression μ_{ion} can be written from Eq.(15) and Eq. (40) as

$$\mu_{\text{ion}} \approx 10^{-4} \left[\left(\frac{\mathcal{F}}{10^5} \right) \left(\frac{10^4}{\kappa} \right) \left(\frac{Z}{26} \right)^3 \left(\frac{56}{A} \right)^2 \right], \quad (41)$$

where \mathcal{F} is the contribution from the integrals involving DF in (15), and Z is the charge of the ions. Firstly, we note that decreasing κ , while formally increasing μ_{ion} , will *not* lead to an increased ion’s contribution to charge separation, because the latter is proportional to $\mu\kappa$ as seen in Eq. (39). Secondly, considering heavier ions is not an option, either, given that $A \propto Z$ and one need to increase μ_{ion} by a factor $\sim 10^4$ to bring it to the size of μ_{\pm} . Thirdly, decreasing the width of the DF so as to boost \mathcal{F} is also not an option as cold plasma approximation is nonphysical for the ion DF.

5 CONCLUSIONS

As previously shown in LMM18, soliton formation in the NLSE with NLD requires small values of the ratio of the NLD to the local cubic nonlinearity, $|s/q| \lesssim 0.1$, and is suppressed for higher values of $|s/q| \gtrsim 0.5$. In this work, motivated by the PSG model, we consider an admixture of electron-positron pairs and ions in the pulsar plasma and derived the NLSE for the envelope of Langmuir waves in the plasma. We found that due to the low density of ions compared to the density of the pair plasma, the ion species contribute negligibly in modifying both the coefficients of the NLSE and the charge separation. For subsequent analysis, we neglected the ions and explored the parameter space of different separation of the electron and positron DF across a wide range of plasma temperatures, obtaining estimates for the range of s/q values and charge separation.

We considered two types of DF: a Lorentzian DF with a prominent power law tail and a Gaussian DF with an exponentially decaying tail. The long-tailed Lorentzian DF provides small values of $|s/q| \sim 0.1$ across a wide range of plasma temperatures for moderate separation of the electron and positron DF. On the other hand, the short-tailed Gaussian DF provides a very restrictive parameter space where small values of $s/q \lesssim 0.1$ can be attained. In reality, the DF can have a tail in between those of a Gaussian and Lorentzian DF. However, as long as DF’s tail falls off “sufficiently slowly” for some extended range of momenta, soliton formation is feasible in pulsar plasma and thus can be considered as a viable candidate to explain occurrence of CCR charge bunches. The radiation pattern due to curvature radiation under hot plasma conditions will be treated in an upcoming work.

ACKNOWLEDGEMENTS

We thank the anonymous referee for useful comments that improved the quality of the manuscript significantly. SMR and DM acknowledge the support of the Department of Atomic Energy, Government of India, under project no. 12-R&D-TFR-5.02-0700. DM acknowledges support and funding from the ‘Indo-French Centre for the Promotion of Advanced Research - CEFIPRA’ grant IFC/F5904-B/2018. This work was supported by the grant 2020/37/B/ST9/02215 of the National Science Centre, Poland.

DATA AVAILABILITY

Simulation data will be made available upon reasonable request from the corresponding author Sk. Minhajur Rahaman.

REFERENCES

- Arendt Paul N. J., Eilek J. A., 2002, *ApJ*, 581, 451
 Arumugasamy P., Mitra D., 2019, *MNRAS*, 489, 4589
 Asseo E., Melikidze G. I., 1998, *MNRAS*, 301, 59
 Basu R., Mitra D., Melikidze G. I., Maciesiak K., Skrzypczak A., Szary A., 2016, *ApJ*, 833, 29
 Blasi P., Amato E., 2011, *Astrophysics and Space Science Proceedings*, 21, 624
 Cheng A. F., Ruderman M. A., 1977, *ApJ*, 212, 800
 Cheng A. F., Ruderman M. A., 1980, *ApJ*, 235, 576
 Daugherty J. K., Harding A. K., 1982, *ApJ*, 252, 337
 Geppert U., 2017, *Journal of Astrophysics and Astronomy*, 38, 46
 Gil J. A., Melikidze G. I., Mitra D., 2002, *A&A*, 388, 235
 Gil J., Melikidze G. I., Geppert U., 2003, *A&A*, 407, 315
 Ginzburg V. L., Zheleznyakov V. V., Zaitsev V. V., 1969, *Ap&SS*, 4, 464
 Goldreich P., Julian W. H., 1969, *ApJ*, 157, 869
 Hibsichman J. A., Arons J., 2001, *ApJ*, 560, 871
 Ichikawa Y. H., 1974, *Progress of Theoretical Physics Supplement*, 55, 212
 Ichikawa Y. H., Taniuti T., 1973, *Journal of the Physical Society of Japan*, 34, 513
 Jordan R., Jossierand C., 2001, *Mathematics and Computers in Simulation*, 55, 433
 Karpman V. I., Normand C. A., Ter Haar D., Tsytovich V. N., 1975, *Phys. Scr.*, 11, 271
 Kazbegi A. Z., Machabeli G. Z., Melikidze G. I., 1991, *MNRAS*, 253, 377
 Kijak J., Gil J., 1997, *MNRAS*, 288, 631
 Kijak J., Gil J., 1998, *MNRAS*, 299, 855
 Lakoba T. I., 2017, *Journal of Scientific Computing*, 72, 14
 Lakoba T., Mitra D., Melikidze G., 2018, *MNRAS*, 480, 4526
 Lighthill M. J., 1967, *Proceedings of the Royal Society of London Series A*, 299, 28
 Lominadze D. G., Machabeli G. Z., Melikidze G. I., Pataraya A. D., 1986, *Fizika Plazmy*, 12, 1233
 Manthei A. C., Benáček J., Muñoz P. A., Büchner J., 2021, *A&A*, 649, A145
 Melikidze G. I., Pataraya A. D., 1978, *Akademiia Nauk Gruzii Soobshcheniia*, 90, 49
 Melikidze G. I., Pataraya A. D., 1980, *Astrofizika*, 16, 161
 Melikidze G. I., Pataraya A. D., 1984, *Astrophysics*, 20, 100
 Melikidze G. I., Gil J. A., Pataraya A. D., 2000, *ApJ*, 544, 1081
 Melrose D. B., 1995, *Journal of Astrophysics and Astronomy*, 16, 137
 Melrose D. B., Gedalin M. E., 1999, *ApJ*, 521, 351
 Mitra D., 2017, *Journal of Astrophysics and Astronomy*, 38, 52
 Mitra D., Li X. H., 2004, *A&A*, 421, 215
 Mitra D., Gil J., Melikidze G. I., 2009, *ApJ*, 696, L141
 Mitra D., Basu R., Melikidze G. I., Arjunwadkar M., 2020, *MNRAS*, 492, 2468
 Pataraya A., Melikidze G., 1980, *Ap&SS*, 68, 49
 Rahaman S. M., Mitra D., Melikidze G. I., 2020, *MNRAS*, 497, 3953
 Rahaman S. k. M., Basu R., Mitra D., Melikidze G. I., 2021, *MNRAS*, 500, 4139
 Ruderman M. A., Sutherland P. G., 1975, *ApJ*, 196, 51
 Sturrock P. A., 1971, *ApJ*, 164, 529
 Suvorov E. V., Chugunov Y. V., 1973, *Ap&SS*, 23, 189
 Szary A., Melikidze G. I., Gil J., 2015, *MNRAS*, 447, 2295

APPENDIX A: DERIVATION OF NLSE WITH NLD

We follow the procedure by Melikidze & Pataraya 1980 (MP80), Pataraya & Melikidze 1980 (PM80), Melikidze & Pataraya 1984 (MP84) and Melikidze et al. 2000 (MGP00) with the addition that arbitrary species α can be included as a plasma component.

We identify two frames of reference. Firstly, we have a Plasma Frame of Reference (hereafter PFR) where the average velocity of the plasma particles is zero. Additionally, we have a Moving Frame of Reference (hereafter MFR) which moves with a velocity $\lambda = v_{\text{gr}}$ with respect to PFR. Here v_{gr} corresponds to the group velocity of the linear plasma waves in PFR. The velocity λ corresponds to the Lorentz factor γ_0 . For simplicity we choose $c = 1$. The transformed quantities are shown in table A1.

We introduce the stretched variables in MFR as

$$\xi' = \epsilon x' \quad (\text{A1})$$

$$\tau' = \epsilon^2 t' \quad (\text{A2})$$

The choice of the stretched variables can be motivated as follows. Consider the dispersion relation and group velocity of Langmuir waves

[h]

Table A1. Transformation of quantities from PFR to MFR

PFR	MFR
x	$x' = \gamma_0(x - \lambda t)$
t	$t' = \gamma_0(t - \lambda x)$
ω	$\omega' = \gamma_0(\omega - k\lambda)$
k	$k' = \gamma_0(k - \lambda\omega)$
p	$p' = \gamma_0(p - \mathcal{E}\lambda)$
v	$v' = \frac{v - \lambda}{1 - \lambda v}$
$v_{\text{gr}} = \frac{d\omega}{dk}$	$v'_{\text{gr}} = \frac{d\omega'}{dk'} = \frac{v_{\text{gr}} - \lambda}{1 - \lambda v_{\text{gr}}}$

in PFR to be defined as

$$\omega = k(1 - \delta_1) \quad (\text{A3})$$

$$\lambda = 1 - \delta_2 \quad (\text{A4})$$

where the quantities $(\delta_1, \delta_2) \ll 1$.

Using the definitions above, the wave quantities (ω, k) in PFR can be transformed to (ω', k') in MFR via the Lorentz transformation as

$$\omega' = \gamma_0(\omega - k\lambda) = \gamma_0 k(\delta_2 - \delta_1) \quad (\text{A5})$$

$$k' = \gamma_0(k - \lambda\omega) = \gamma_0 k(\delta_2 + \delta_1) \quad (\text{A6})$$

Thus, the transformed wave varies much slower in time compared to variation in space. Hence, it justifies the choice of stretched time variable to be second order in ϵ and the stretched space variable to be first order in ϵ .

Making use of the stretched variables we have

$$\frac{\partial}{\partial t'} \rightarrow \frac{\partial}{\partial t'} + \frac{\partial \tau'}{\partial t'} \frac{\partial}{\partial \tau'} \rightarrow \frac{\partial}{\partial t'} + \epsilon^2 \frac{\partial}{\partial \tau'} \quad (\text{A7})$$

$$\frac{\partial}{\partial x'} \rightarrow \frac{\partial}{\partial x'} + \frac{\partial \xi'}{\partial x'} \frac{\partial}{\partial \xi'} \rightarrow \frac{\partial}{\partial x'} + \epsilon \frac{\partial}{\partial \xi'} \quad (\text{A8})$$

We define the particle distribution function and the electric field in MFR as

$$f'_{\alpha} = f^{(0)'}(p') + \sum_{l=-\infty}^{+\infty} \sum_{n=1}^{+\infty} \epsilon^n e^{il(k'x' - \omega't')} f_{\alpha,l}^{(n)'}(p', \xi', \tau') \quad (\text{A9})$$

$$E = \sum_{l=-\infty}^{+\infty} \sum_{n=1}^{+\infty} \epsilon^n e^{il(k'x' - \omega't')} E_l^{(n)}(\xi', \tau') \quad (\text{A10})$$

where the stretched variable amplitudes are given by

$$f_{\alpha,l}^{(n)'} = \frac{1}{2\pi} \int d\Omega' \int dK' \exp i(K'\xi' - \Omega'\tau') \tilde{f}_{\alpha,l}^{(n)'}(p', \Omega', K') \quad (\text{A11})$$

$$E_l^{(n)} = \frac{1}{2\pi} \int d\Omega' \int dK' \exp i(K'\xi' - \Omega'\tau') \tilde{E}_l^{(n)}(\Omega', K') \quad (\text{A12})$$

subject to the reality condition

$$E_l^{(n)\star} = E_{-l}^{(n)} \quad (\text{A13})$$

$$f_{\alpha,l}^{(n)\star} = f_{\alpha,-l}^{(n)} \quad (\text{A14})$$

Using equation (A7) and equation (A8) the Vlasov Equation in MFR takes the form

$$\frac{\partial f'_{\alpha}}{\partial t'} + v' \frac{\partial f'_{\alpha}}{\partial x'} + \frac{e_{\alpha} E}{m_{\alpha}} \frac{\partial f'_{\alpha}}{\partial p'} = 0$$

$$\Rightarrow \left[\frac{\partial f'_{\alpha}}{\partial t'} + \epsilon^2 \frac{\partial f'_{\alpha}}{\partial \tau'} \right] + v' \left[\frac{\partial f'_{\alpha}}{\partial x'} + \epsilon \frac{\partial f'_{\alpha}}{\partial \xi'} \right] + \left(\frac{e_{\alpha} E}{m_{\alpha}} \right) \frac{\partial f'_{\alpha}}{\partial p'} = 0$$

Using equation (A9) and equation (A10) in the equation above the Master equation for Vlasov Equation (hereafter MVE) is

$$il(\omega' - k'v') f_{\alpha,l}^{(n)'} - \frac{\partial f_{\alpha,l}^{(n-2)'}}{\partial \tau'} - v' \frac{\partial f_{\alpha,l}^{(n-1)'}}{\partial \xi'} = \frac{e_{\alpha}}{m_{\alpha}} \left[E_l^{(n)} \frac{\partial f_{\alpha}^{(0)'}}{\partial p'} + \sum_{j=-\infty}^{+\infty} \sum_{m=1}^{+\infty} \frac{\partial f_{\alpha,j}^{(m)'}}{\partial p'} E_{l-j}^{(n-m)} \right] \quad (\text{A15})$$

Using equation (A8) the Poisson's equation in MFR is written as

$$\begin{aligned} \frac{\partial E}{\partial x'} &= 4\pi \sum_{\alpha} e_{\alpha} n'_{\alpha} \int_{-\infty}^{+\infty} dp' f'_{\alpha} \\ \Rightarrow \left[\frac{\partial}{\partial x'} + \epsilon \frac{\partial}{\partial \xi'} \right] E &= 4\pi \sum_{\alpha} n'_{\alpha} e_{\alpha} \int_{-\infty}^{+\infty} dp' f'_{\alpha} \end{aligned}$$

Using equation (A9) and equation (A10) in the equation above the Master equation for Poisson's equation (hereafter MPE) in MFR is

$$ik' E_l^{(n)} + \frac{\partial E_l^{(n-1)}}{\partial \xi'} = 4\pi \sum_{\alpha} n'_{\alpha} e_{\alpha} \int_{-\infty}^{+\infty} dp' f_{\alpha,l}^{(n)'} \quad (\text{A16})$$

A1 $n=1, l=1$ term

From MVE we get,

$$f_{\alpha,1}^{(1)'} = \frac{G'_{\alpha}}{i(\omega' - k'v')} E_1^{(1)} \quad (\text{A17})$$

where

$$G'_{\alpha} = \frac{e_{\alpha}}{m_{\alpha}} \frac{\partial f_{\alpha}^{(0)'}}{\partial p'} \quad (\text{A18})$$

From MPE we have,

$$k' + \sum_{\alpha} \omega_{p,\alpha}^2 \int_{-\infty}^{+\infty} dp' \frac{\partial f_{\alpha}^{(0)'}}{\partial p'} \frac{1}{(\omega' - k'v')} = 0 \quad (\text{A19})$$

where

$$\omega_{p,\alpha}^2 = \frac{4\pi n'_{\alpha} e_{\alpha}^2}{m_{\alpha}} \quad (\text{A20})$$

In what follow in each subsection the MPE and MVE term corresponding to a set (n, l) is evaluated. Each term becomes an input to the next term until at $n = 3, l = 1$ we obtain the NLSE governing the envelope electric field $E_1^{(1)}$.

A2 $n = 1, l = 0$ term

Substituting $(n = 1, l = 0)$ in MVE we have,

$$E_0^{(1)} = 0 \quad (\text{A21})$$

Substituting $(n = 1, l = 0)$ in MPE we have,

$$4\pi \sum_{\alpha} n'_{\alpha} e_{\alpha} \int_{-\infty}^{+\infty} dp' f_{\alpha,0}^{(1)'} = 0 \quad (\text{A22})$$

A2.1 $n = 2, l = 0$ term

Substituting $(n = 2, l = 0)$ in MVE we get,

$$v' \frac{\partial f_{\alpha,0}^{(1)'}}{\partial \xi'} = -\frac{e_{\alpha}}{m_{\alpha}} \left[E_0^{(2)} \frac{\partial f_{\alpha}^{(0)'}}{\partial p'} + \left\{ E_{-1}^{(1)} \frac{\partial f_{\alpha,1}^{(1)'}}{\partial p'} + E_1^{(1)} \frac{\partial f_{\alpha,-1}^{(1)'}}{\partial p'} \right\} \right] \quad (\text{A23})$$

Now using A1 we have

$$E_{-1}^{(1)} \frac{\partial f_{\alpha,1}^{(1)'}}{\partial p'} + E_1^{(1)} \frac{\partial f_{\alpha,-1}^{(1)'}}{\partial p'} = - \left[|E_1^{(1)}|^2 \frac{\partial}{\partial p'} \left\{ \frac{G'_{\alpha}}{i(\omega' - k'v')} \right\} - |E_1^{(1)}|^2 \frac{\partial}{\partial p'} \left\{ \frac{G'_{\alpha}}{i(\omega' - k'v')} \right\} \right] = 0 \quad (\text{A24})$$

Substituting equation (A51) in equation (A23) we get

$$\frac{\partial f_{\alpha,0}^{(1)'}}{\partial \xi'} = -\frac{e_{\alpha}}{m_{\alpha}} \frac{1}{v'} \frac{\partial f_{\alpha}^{(0)'}}{\partial p'} E_0^{(2)} \quad (\text{A25})$$

Substituting equation (A11) in equation (A26) we get

$$\tilde{f}_{\alpha,0}^{(1)} = -\frac{1}{iK'} \frac{e_\alpha}{m_\alpha} \frac{1}{v'} \frac{\partial f_\alpha^{(0)'}}{\partial p'} \tilde{E}_0^{(2)} \quad (\text{A26})$$

Using equation (A26) in equation (A22) we get,

$$4\pi \sum_\alpha n'_\alpha e_\alpha \int_{-\infty}^{+\infty} dp \tilde{f}_{\alpha,0}^{(1)} = 0 \Rightarrow \left\{ \sum_\alpha \omega_{p,\alpha}^2 \int_{-\infty}^{+\infty} dp' \frac{1}{v'} \frac{\partial f_\alpha^{(0)'}}{\partial p'} \right\} \tilde{E}_0^{(2)} = 0 \quad (\text{A27})$$

which gives

$$\tilde{E}_0^{(2)} = 0 \quad (\text{A28})$$

Using equation (A28) in equation (A26) we have

$$\tilde{f}_{\alpha,0}^{(1)' } = 0 \quad (\text{A29})$$

Using equation (A29) and equation (A28) we have

$$E_0^{(2)} = 0 \quad (\text{A30})$$

$$f_{\alpha,0}^{(1)' } = 0 \quad (\text{A31})$$

A3 $n=1, l \neq 0$ term

Substituting ($n = 1, l \neq 0$) in MVE we have

$$f_{\alpha,l}^{(1)' } = \frac{G'_\alpha}{i l (\omega' - k' v')} E_l^{(1)} \quad (\text{A32})$$

Substituting ($n = 1, l \neq 0$) in MPE,

$$\begin{aligned} ik' E_1^{(1)} &= 4\pi \sum_\alpha n'_\alpha e_\alpha \int_{-\infty}^{+\infty} dp' f_{\alpha,l}^{(1)' } \\ \Rightarrow \left[k' + l^2 \sum_\alpha \omega_{p,\alpha}^2 \int_{-\infty}^{+\infty} dp' \frac{\partial f_\alpha^{(0)'}}{\partial p'} \frac{1}{(\omega' - k' v')} \right] E_l^{(1)} &= 0 \\ \Rightarrow (1 - l^2) E_l^{(1)} &= 0 \end{aligned}$$

To summarize we have

$$E_l^{(1)} = 0 \quad \text{for } |l| > 1 \quad (\text{A33})$$

$$f_{\alpha,l}^{(1)' } = 0 \quad \text{for } |l| > 1 \quad (\text{A34})$$

A4 $n = 2, l = 1$ term

Substituting ($n = 2, l = 1$) in MVE we have,

$$f_{\alpha,1}^{(2)' } = \frac{1}{i(\omega' - k' v')} \left[G'_\alpha E_1^{(2)} + v' \frac{\partial f_{\alpha,1}^{(1)'}}{\partial \xi'} \right] \quad (\text{A35})$$

Substituting ($n = 2, l = 1$) in MPE we have,

$$\begin{aligned} ik' E_1^{(2)} + \frac{\partial E_1^{(1)}}{\partial \xi'} &= 4\pi \sum_\alpha n'_\alpha e_\alpha \int_{-\infty}^{+\infty} dp' f_{\alpha,1}^{(2)' } \\ \Rightarrow i \left[k' + \sum_\alpha \omega_{p,\alpha}^2 \int_{-\infty}^{+\infty} dp' \frac{\partial f_\alpha^{(0)'}}{\partial p'} \frac{1}{(\omega' - k' v')} \right] E_1^{(2)} + \frac{\partial E_1^{(1)}}{\partial \xi'} &= 4\pi \sum_\alpha n'_\alpha e_\alpha \int_{-\infty}^{+\infty} dp' \frac{v'}{i(\omega' - k' v')} \frac{\partial f_{\alpha,1}^{(1)'}}{\partial \xi'} \\ \Rightarrow \left[1 + \sum_\alpha \omega_{p,\alpha}^2 \int_{-\infty}^{+\infty} dp \frac{v'}{(\omega' - k' v')^2} \frac{\partial f_\alpha^{(0)'}}{\partial p'} \right] \frac{\partial E_1^{(1)}}{\partial \xi'} &= 0 \end{aligned}$$

The condition given above is referred to as the solvability condition. This requires that the term in the square brackets be zero.

We differentiate equation (A19) with respect to k' to obtain

$$1 + \sum_{\alpha} \omega_{p,\alpha}^2 \int_{-\infty}^{+\infty} dp' \frac{1}{(\omega' - k'v')^2} \left\{ - \left(\frac{d\omega'}{dk'} - v' \right) \right\} \frac{\partial f_{\alpha}^{(0)'}}{\partial p'} = 0 \quad (\text{A36})$$

Thus, the solvability condition requires the group velocity of the transformed waves in MFR to be zero

$$v'_{\text{gr}} = \frac{d\omega'}{dk'} = 0 \Rightarrow \frac{v_{\text{gr}} - \lambda}{1 - \lambda v_{\text{gr}}} = 0 \Rightarrow \lambda = v_{\text{gr}} = \frac{d\omega}{dk} \quad (\text{A37})$$

Thus, the solvability condition is satisfied since the velocity of MFR has been identified with the group velocity of the linear Langmuir waves in PFR.

A5 $n = 2, l = 2$ term

Substituting ($n = 2, l = 2$) in MVE and using Eq. A23 we get,

$$\begin{aligned} & i2(\omega' - k'v')f_{\alpha,2}^{(2)'} \\ &= \frac{e_{\alpha}}{m_{\alpha}} \left[E_2^{(2)} \frac{\partial f_{\alpha}^{(0)'}}{\partial p'} + \sum_{j=-\infty}^{+\infty} \sum_{m=1}^{+\infty} \frac{\partial f_{\alpha,j}^{(m)'}}{\partial p'} E_{2-j}^{(2-m)} \right] \\ &= \frac{e_{\alpha}}{m_{\alpha}} \left[E_2^{(2)} \frac{\partial f_{\alpha}^{(0)'}}{\partial p'} + \sum_{j=-\infty}^{+\infty} \frac{\partial f_{\alpha,j}^{(1)'}}{\partial p'} E_{2-j}^{(1)} \right] \\ &= \frac{e_{\alpha}}{m_{\alpha}} \left[E_2^{(2)} \frac{\partial f_{\alpha}^{(0)'}}{\partial p'} + \frac{\partial f_{\alpha,1}^{(1)'}}{\partial p'} E_1^{(1)} \right] \end{aligned}$$

which gives

$$f_{\alpha,2}^{(2)'} = \frac{1}{2i} \frac{e_{\alpha}}{m_{\alpha}} \frac{1}{(\omega' - k'v')} \left[E_2^{(2)} \frac{\partial f_{\alpha}^{(0)'}}{\partial p'} + E_1^{(1)} \frac{\partial f_{\alpha,1}^{(1)'}}{\partial p'} \right] \quad (\text{A38})$$

Substituting ($n = 2, l = 2$) in MPE we have,

$$\begin{aligned} & 2ik' E_2^{(2)} = 4\pi \sum_{\alpha} n'_{\alpha} e_{\alpha} \int_{-\infty}^{+\infty} dp' f_{\alpha,2}^{(2)'} \\ \Rightarrow & \left[2ik' - \frac{1}{2i} \sum_{\alpha} \omega_{p,\alpha}^2 \int_{-\infty}^{+\infty} dp' \frac{1}{(\omega' - k'v')} \frac{\partial f_{\alpha}^{(0)'}}{\partial p'} \right] E_2^{(2)} = \frac{1}{2i} \sum_{\alpha} \omega_{p,\alpha}^2 \int_{-\infty}^{+\infty} dp' \frac{1}{(\omega' - k'v')} \frac{\partial f_{\alpha,1}^{(1)'}}{\partial p'} \\ \Rightarrow & -\frac{3k'}{2i} E_2^{(2)} = \frac{1}{2i} \sum_{\alpha} \omega_{p,\alpha}^2 \int_{-\infty}^{+\infty} dp' \frac{1}{(\omega' - k'v')} \frac{\partial f_{\alpha,1}^{(1)'}}{\partial p'} \\ \Rightarrow & -\frac{3k'}{2i} E_2^{(2)} = \frac{1}{2i} \sum_{\alpha} \omega_{p,\alpha}^2 \int_{-\infty}^{+\infty} dp' \frac{1}{(\omega' - k'v')} \frac{\partial}{\partial p'} \left\{ \frac{G'_{\alpha}}{i(\omega' - k'v')} \right\} E_1^{(1)^2} \end{aligned}$$

which finally gives

$$E_2^{(2)} = \frac{i}{3k'} A E_1^{(1)^2} \quad (\text{A39})$$

where

$$A = \sum_{\alpha} \omega_{p,\alpha}^2 \int_{-\infty}^{+\infty} dp' \frac{1}{(\omega' - k'v')} \frac{\partial}{\partial p'} \left\{ \frac{e_{\alpha}}{m_{\alpha}} \frac{\partial f_{\alpha}^{(0)'}}{\partial p'} \frac{1}{(\omega' - k'v')} \right\} \quad (\text{A40})$$

A6 $n = 3, l = 0$ term

Substituting ($n = 3, l = 0$) in MVE we get,

$$\begin{aligned} & v' \frac{\partial f_{\alpha,0}^{(2)'}}{\partial \xi'} \\ &= -\frac{e_\alpha}{m_\alpha} \left[E_0^{(3)} \frac{\partial f_\alpha^{(0)'}}{\partial p'} + \sum_{j=-\infty}^{+\infty} \sum_{m=1}^{+\infty} \frac{\partial f_{\alpha,j}^{(m)'}}{\partial p} E_{-j}^{(1)} \right] \\ &= -\frac{e_\alpha}{m_\alpha} \left[E_0^{(3)} \frac{\partial f_\alpha^{(0)'}}{\partial p'} + \sum_{j=-\infty}^{+\infty} \left\{ \frac{\partial f_{\alpha,j}^{(1)'}}{\partial p'} E_{-j}^{(2)} + \frac{\partial f_{\alpha,j}^{(2)'}}{\partial p'} E_{-j}^{(1)} \right\} \right] \\ &= -\frac{e_\alpha}{m_\alpha} \left[E_0^{(3)} \frac{\partial f_\alpha^{(0)'}}{\partial p'} + E_{-1}^{(2)} \frac{\partial f_{\alpha,1}^{(1)'}}{\partial p'} + E_1^{(2)} \frac{\partial f_{\alpha,-1}^{(1)'}}{\partial p'} + E_{-1}^{(1)} \frac{\partial f_{\alpha,1}^{(2)'}}{\partial p} + E_1^{(1)} \frac{\partial f_{\alpha,-1}^{(2)'}}{\partial p} \right] \end{aligned}$$

which finally gives

$$v' \frac{\partial f_{\alpha,0}^{(2)'}}{\partial \xi'} = -\frac{e_\alpha}{m_\alpha} \left[E_0^{(3)} \frac{\partial f_\alpha^{(0)'}}{\partial p'} + E_{-1}^{(2)} \frac{\partial f_{\alpha,1}^{(1)'}}{\partial p'} + E_{-1}^{(2)*} \frac{\partial f_{\alpha,-1}^{(1)'}}{\partial p'} + E_{-1}^{(1)} \frac{\partial f_{\alpha,1}^{(2)'}}{\partial p} + E_{-1}^{(1)*} \frac{\partial f_{\alpha,-1}^{(2)'}}{\partial p} \right] \quad (\text{A41})$$

From equation (A35) we have,

$$f_{\alpha,1}^{(2)'} = \frac{1}{i(\omega' - k'v')} \left[G'_\alpha E_1^{(2)} + v' \frac{\partial f_{\alpha,1}^{(1)'}}{\partial \xi'} \right] = \frac{G'_\alpha}{i(\omega' - k'v')} E_1^{(2)} + \frac{v'}{i(\omega' - k'v')} \frac{\partial f_{\alpha,1}^{(1)'}}{\partial \xi'} \quad (\text{A42})$$

which gives

$$E_{-1}^{(1)} \frac{\partial f_{\alpha,1}^{(2)'}}{\partial p'} = \frac{|E_1^{(1)}|^2}{E_1^{(1)2}} E_1^{(2)} \frac{\partial f_{\alpha,1}^{(1)'}}{\partial p'} + E_{-1}^{(1)} \frac{\partial}{\partial p'} \left[\frac{v'}{i(\omega' - k'v')} \frac{\partial f_{\alpha,1}^{(1)'}}{\partial \xi'} \right] \quad (\text{A43})$$

$$E_1^{(1)} \frac{\partial f_{\alpha,-1}^{(2)'}}{\partial p'} = \frac{|E_1^{(1)}|^2}{E_1^{(1)2}} E_{-1}^{(2)} \frac{\partial f_{\alpha,-1}^{(1)'}}{\partial p'} - E_1^{(1)} \frac{\partial}{\partial p'} \left[\frac{v'}{i(\omega' - k'v')} \frac{\partial f_{\alpha,-1}^{(1)'}}{\partial \xi'} \right] \quad (\text{A44})$$

Using equation (A43) and (A44) in equation (A41)

$$\begin{aligned} v' \frac{\partial f_{\alpha,0}^{(2)'}}{\partial \xi'} &= -\frac{e_\alpha}{m_\alpha} \left[E_0^{(3)} \frac{\partial f_\alpha^{(0)'}}{\partial p'} + \left\{ \frac{|E_1^{(1)}|^2}{E_1^{(1)2}} E_1^{(2)} + E_{-1}^{(2)} \right\} \frac{\partial f_{\alpha,1}^{(1)'}}{\partial p'} + \left\{ \frac{|E_1^{(1)}|^2}{E_1^{(1)2}} E_{-1}^{(2)} + E_1^{(2)} \right\} \frac{\partial f_{\alpha,-1}^{(1)'}}{\partial p'} \right] \\ &- \frac{e_\alpha}{m_\alpha} E_{-1}^{(1)} \frac{\partial}{\partial p'} \left[\frac{v'}{i(\omega' - k'v')} \frac{\partial f_{\alpha,1}^{(1)'}}{\partial \xi'} \right] + \frac{e_\alpha}{m_\alpha} E_1^{(1)} \frac{\partial}{\partial p'} \left[\frac{v'}{i(\omega' - k'v')} \frac{\partial f_{\alpha,-1}^{(1)'}}{\partial \xi'} \right] \end{aligned} \quad (\text{A45})$$

Next we simplify

$$\begin{aligned} & \left\{ \frac{|E_1^{(1)}|^2}{E_1^{(1)2}} E_1^{(2)} + E_{-1}^{(2)} \right\} \frac{\partial f_{\alpha,1}^{(1)'}}{\partial p'} = \left[E_1^{(2)} E_1^{(1)} + E_1^{(2)} \frac{|E_1^{(1)}|^2}{E_1^{(1)}} \right] \frac{\partial}{\partial p'} \left\{ \frac{G'_\alpha}{i(\omega' - k'v')} \right\}, \\ & \left\{ \frac{|E_1^{(1)}|^2}{E_1^{(1)2}} E_{-1}^{(2)} + E_1^{(2)} \right\} \frac{\partial f_{\alpha,-1}^{(1)'}}{\partial p'} = - \left[E_1^{(2)} E_1^{(1)*} + E_1^{(2)*} \frac{|E_1^{(1)}|^2}{E_1^{(1)*}} \right] \frac{\partial}{\partial p'} \left\{ \frac{G'_\alpha}{i(\omega' - k'v')} \right\} \end{aligned}$$

which gives us

$$\left\{ \frac{|E_1^{(1)}|^2}{E_1^{(1)2}} E_1^{(2)} + E_{-1}^{(2)} \right\} \frac{\partial f_{\alpha,1}^{(1)'}}{\partial p'} + \left\{ \frac{|E_1^{(1)}|^2}{E_1^{(1)2}} E_{-1}^{(2)} + E_1^{(2)} \right\} \frac{\partial f_{\alpha,-1}^{(1)'}}{\partial p'} = 0 \quad (\text{A46})$$

Next we simplify

$$E_{-1}^{(1)} \frac{\partial X'}{\partial p'} \left[\frac{v'}{i(\omega' - k'v')} \frac{\partial f_{\alpha,1}^{(1)'}}{\partial \xi'} \right] = - \frac{\partial}{\partial p'} \left\{ \frac{v' G'_\alpha}{(\omega' - k'v')^2} \right\} E_1^{(1)*} \frac{\partial E_1^{(1)}}{\partial \xi'} = - I'_\alpha \left\{ \frac{\partial}{\partial \xi'} |E_1^{(1)}|^2 - E_1^{(1)} \frac{\partial E_1^{(1)}}{\partial \xi'} \right\} \quad (\text{A47})$$

where

$$I'_\alpha = \frac{\partial}{\partial p'} \left\{ \frac{v' G'_\alpha}{(\omega' - k'v')^2} \right\} \quad (\text{A48})$$

Similarly we have,

$$E_1^{(1)} \frac{\partial Y'}{\partial p'} \left[\frac{v'}{i(\omega' - k'v')} \frac{\partial f_{\alpha,-1}^{(1)'}}{\partial \xi'} \right] = I'_\alpha E_1^{(1)} \frac{\partial E_1^{(1)\star}}{\partial \xi'} \quad (\text{A49})$$

Substituting equation (A46) - (A49) in equation(A45)

$$\frac{\partial f_{\alpha,0}^{(2)'}}{\partial \xi'} = -\frac{1}{v'} \left[E_0^{(3)} G'_\alpha - \frac{e_\alpha}{m_\alpha} I'_\alpha \frac{\partial}{\partial \xi'} |E_1^{(1)}|^2 \right] \quad (\text{A50})$$

A7 $n = 2, l = 0$ term

Substituting ($n = 2, l = 0$) in MPE we have

$$\begin{aligned} 4\pi \sum_\alpha n'_\alpha e_\alpha \int_{-\infty}^{+\infty} dp' f_{\alpha,0}^{(2)'} &= 0 \\ \Rightarrow \sum_\alpha \omega_{p,\alpha}^{\prime 2} \int_{-\infty}^{+\infty} dp' \frac{\partial f_{\alpha,0}^{(2)'}}{\partial \xi'} &= 0 \\ \Rightarrow \left\{ \sum_\alpha \omega_{p,\alpha}^{\prime 2} \int_{-\infty}^{+\infty} dp' \frac{1}{v'} \frac{\partial f_{\alpha,0}^{(0)'}}{\partial p'} \right\} E_0^{(3)} &= \left\{ \sum_\alpha \omega_{p,\alpha}^{\prime 2} \int_{-\infty}^{+\infty} dp' \frac{I'_\alpha}{v'} \right\} \frac{\partial}{\partial \xi'} |E_1^{(1)}|^2 \end{aligned}$$

which gives

$$E_0^{(3)} = \frac{\zeta'}{\Delta'} \frac{\partial}{\partial \xi'} |E_1^{(1)}|^2 \quad (\text{A51})$$

Substituting equation (A51) in equation (A50) we get,

$$\frac{\partial f_{\alpha,0}^{(2)'}}{\partial \xi'} = -\frac{K'}{K'v'} \left[\frac{\zeta'}{\Delta'} G'_\alpha - \left(\frac{e_\alpha}{m_\alpha} I'_\alpha \right) \right] \frac{\partial}{\partial \xi'} |E_1^{(1)}|^2 \quad (\text{A52})$$

Using (A11) and (A12) in

$$f_{\alpha,0}^{(2)'} = -\frac{1}{v'} \left[\frac{\zeta'}{\Delta'} G'_\alpha - \left(\frac{e_\alpha}{m_\alpha} I'_\alpha \right) \right] |E_1^{(1)}|^2 \quad (\text{A53})$$

Here Δ' is given by

$$\begin{aligned} \Delta' &= \lim_{\mu \rightarrow 0} \sum_\alpha \omega_{p,\alpha}^{\prime 2} \int_{-\infty}^{+\infty} dp' \frac{K'}{K'v' + i\mu} \frac{\partial f_{\alpha,0}^{(0)'}}{\partial p'} \\ &= \sum_\alpha \omega_{p,\alpha}^{\prime 2} \mathcal{P} \int_{-\infty}^{+\infty} dp' \frac{1}{v'} \frac{\partial f_{\alpha,0}^{(0)'}}{\partial p'} - i\pi \sum_\alpha \omega_{p,\alpha}^{\prime 2} \int_{-\infty}^{+\infty} dp' \frac{K'}{|K'|} \delta(v') \frac{\partial f_{\alpha,0}^{(0)'}}{\partial p'} \end{aligned}$$

which gives

$$\Delta' = H - i U \operatorname{sgn}(K') \quad (\text{A54})$$

where

$$\operatorname{sgn}(K') = \frac{K'}{|K'|} \quad (\text{A55})$$

$$H = \sum_\alpha \omega_{p,\alpha}^{\prime 2} \mathcal{P} \int_{-\infty}^{+\infty} dp' \frac{1}{v'} \frac{\partial f_{\alpha,0}^{(0)'}}{\partial p'} \quad (\text{A56})$$

$$U = \pi \sum_\alpha \omega_{p,\alpha}^{\prime 2} \int_{-\infty}^{+\infty} dp' \delta(v') \frac{\partial f_{\alpha,0}^{(0)'}}{\partial p'} \quad (\text{A57})$$

where \mathcal{P} stands for the Principal value integral. Here and in what follows we will assume μ to be positive following the prescription by Ichikawa 1974.

Next we have ζ' which can be expressed as

$$\zeta' = \lim_{\mu \rightarrow 0} \sum_\alpha \omega_{p,\alpha}^{\prime 2} \int_{-\infty}^{+\infty} dp' \frac{K'}{K'v' + i\mu} \frac{dv'}{dp'} \frac{1}{(\omega' - k'v')^2} G'_\alpha \quad (\text{A58})$$

which gives

$$\zeta' = W - i V \operatorname{sgn}(K') \quad (\text{A59})$$

where

$$W = \sum_{\alpha} \omega_{p,\alpha}^2 \mathcal{P} \int_{-\infty}^{+\infty} dp' \frac{1}{v'} \frac{dv'}{dp'} \frac{1}{(\omega' - k'v')^2} \left\{ \frac{e_{\alpha}}{m_{\alpha}} \frac{\partial f_{\alpha}^{(0)'}}{\partial p'} \right\} \quad (\text{A60})$$

$$V = \pi \sum_{\alpha} \omega_{p,\alpha}^2 \int_{-\infty}^{+\infty} dp' \delta(v') \frac{dv'}{dp'} \frac{1}{(\omega' - k'v')^2} \left\{ \frac{e_{\alpha}}{m_{\alpha}} \frac{\partial f_{\alpha}^{(0)'}}{\partial p'} \right\} \quad (\text{A61})$$

A8 $n = 3, l = 1$ term

Substituting ($n = 3, l = 1$) in MVE we have,

$$f_{\alpha,1}^{(3)'} = \frac{1}{i(\omega' - k'v')} \frac{\partial f_{\alpha,1}^{(1)'}}{\partial \tau'} + \frac{(v')}{i(\omega' - k'v')} \frac{\partial f_{\alpha,1}^{(2)'}}{\partial \xi'} \\ + \frac{1}{i(\omega' - k'v')} \frac{e_{\alpha}}{m_{\alpha}} \left[E_1^{(3)} \frac{\partial f_{\alpha}^{(0)'}}{\partial p'} + E_2^{(2)} \frac{\partial f_{\alpha,-1}^{(1)'}}{\partial p'} + E_1^{(1)} \frac{\partial f_{\alpha,0}^{(2)'}}{\partial p'} + E_{-1}^{(1)} \frac{\partial f_{\alpha,2}^{(2)'}}{\partial p'} \right] \quad (\text{A62})$$

From MPE we get,

$$ik' E_1^{(3)} + \frac{\partial E_1^{(2)}}{\partial \xi'} = 4\pi \sum_{\alpha} n'_{\alpha} e_{\alpha} \int_{-\infty}^{+\infty} dp' f_{\alpha,1}^{(3)'}, \quad (\text{A63})$$

Substituting equation (A62) in equation (A63) we get,

$$ik' E_1^{(3)} + \frac{\partial E_1^{(2)}}{\partial \xi'} = I_1 + I_2 + I_3 + I_4 + I_5 + I_6, \quad (\text{A64})$$

Simplification of Integrals ($I_1 - I_6$)

We can simplify I_1 as

$$I_1 = E_1^{(3)} \sum_{\alpha} \omega_{p,\alpha}^2 \int_{-\infty}^{+\infty} dp' \frac{1}{i(\omega' - k'v')} \frac{\partial f_{\alpha}^{(0)'}}{\partial p'} = ik' E_1^{(3)},$$

We can simplify I_2 using

$$I_2 = 4\pi \sum_{\alpha} n'_{\alpha} e_{\alpha} \int_{-\infty}^{+\infty} dp' \frac{1}{i(\omega' - k'v')} \frac{\partial f_{\alpha,1}^{(1)'}}{\partial \tau'} = \left(\frac{2k'}{\omega'} \right) \frac{\partial E_1^{(1)}}{\partial \tau'}, \quad (\text{A65})$$

We can simplify I_3 as

$$I_3 = 4\pi \sum_{\alpha} n'_{\alpha} e_{\alpha} \int_{-\infty}^{+\infty} dp' \frac{(v' - v'_{gr})}{i(\omega' - k'v')} \frac{\partial f_{\alpha,1}^{(2)'}}{\partial \xi'} = \frac{\partial E_1^{(2)}}{\partial \xi'} - i \frac{1}{2} \frac{d^2 \omega'}{dk'^2} \left(\frac{2k'}{\omega'} \right) \frac{\partial^2 E_1^{(1)}}{\partial \xi'^2}, \quad (\text{A66})$$

We can simplify I_4 as

$$I_4 = \sum_{\alpha} \omega_{p,\alpha}^2 \int_{-\infty}^{+\infty} dp' \frac{1}{i(\omega' - k'v')} \left\{ E_2^{(2)} \frac{\partial f_{\alpha,-1}^{(1)'}}{\partial p'} \right\} = \frac{iA^2}{3k'} |E_1^{(1)}|^2 E_1^{(1)}, \quad (\text{A67})$$

We can simplify I_5 as

$$I_5 = \sum_{\alpha} \omega_{p,\alpha}^2 \int_{-\infty}^{+\infty} dp' \frac{1}{i(\omega' - k'v')} \left\{ E_1^{(1)*} \frac{\partial f_{\alpha,2}^{(2)'}}{\partial p'} \right\} = -i \left(\frac{A^2}{6k'} - \frac{B}{2} \right) |E_1^{(1)}|^2 E_1^{(1)}, \quad (\text{A68})$$

where

$$B = \sum_{\alpha} \omega_{p,\alpha}^2 \int_{-\infty}^{+\infty} dp' \frac{1}{(\omega' - k'v')} \left(\frac{e_{\alpha}}{m_{\alpha}} \right)^2 \frac{\partial}{\partial p'} \left[\frac{1}{(\omega' - k'v')} \frac{\partial}{\partial p'} \left\{ \frac{\partial f_{\alpha}^{(0)'}}{\partial p'} \frac{1}{(\omega' - k'v')} \right\} \right] \quad (\text{A69})$$

We can simplify I_6 as

$$\begin{aligned}
 I_6 &= \sum_{\alpha} \omega_{p,\alpha}^2 \int_{-\infty}^{+\infty} dp' \frac{1}{(\omega' - k'v')} \frac{\partial f_{\alpha,0}^{(2)'}}{\partial p'} \\
 &= k' \left(\frac{\xi'^2}{\Delta'} - \Lambda' \right) |E_1^{(1)}|^2 \\
 &= k' \left(\left\{ \frac{H(W^2 - V^2) + 2WVU}{H^2 + U^2} + C \right\} + i \left\{ \frac{U(W^2 - V^2) - 2WVH}{H^2 + U^2} + D \right\} \text{sgn}(K') \right) |E_1^{(1)}|^2 \\
 &= k' \Theta |E_1^{(1)}|^2 + i k' \Phi \left\{ \text{sgn}(K') |E_1^{(1)}|^2 \right\} \\
 &= k' \Theta |E_1^{(1)}|^2 + i k' \Phi \left\{ \text{sgn}(K') \right\} |E_1^{(1)}|^2 \\
 &= k' \Theta |E_1^{(1)}|^2 + i k' \Phi \left\{ \int_{-\infty}^{+\infty} d\xi' e^{-iK'\xi'} \frac{1}{i\pi\xi'} \right\} |E_1^{(1)}|^2 \\
 &= k' \Theta |E_1^{(1)}|^2 + i k' \Phi \left\{ \int_{-\infty}^{+\infty} d\xi' e^{-iK'\xi'} |E_1^{(1)}(\xi', \tau')|^2 \times \frac{1}{i\pi\xi'} \right\} \\
 &= k' \Theta |E_1^{(1)}|^2 + k' \Phi \frac{1}{\pi} \left(|E_1^{(1)}(\xi', \tau')|^2 \otimes \frac{1}{\xi'} \right) \\
 &= k' \Theta |E_1^{(1)}|^2 + k' \Phi \frac{1}{\pi} \left\{ \mathcal{P} \int_{-\infty}^{+\infty} d\xi'' \frac{|E_1^{(1)}(\xi'', \tau')|^2}{\xi' - \xi''} \right\}
 \end{aligned}$$

where we have,

$$\Theta'(\omega', k') = \left\{ \frac{H(W^2 - V^2) + 2WVU}{H^2 + U^2} + C \right\} \quad (\text{A70})$$

$$\Phi'(\omega', k') = \left\{ \frac{U(W^2 - V^2) - 2WVH}{H^2 + U^2} + D \right\} \quad (\text{A71})$$

Substituting I_1 to I_6 in equation (A62) we have

$$- \left(\frac{2k'}{\omega'} \right) i \frac{\partial E_1^{(1)}}{\partial \tau'} - \frac{1}{2} \frac{d^2 \omega'}{dk'^2} \left(\frac{2k'}{\omega'} \right) \frac{\partial^2 E_1^{(1)}}{\partial \xi'^2} + \left[\left(\frac{A^2}{6k'} + \frac{B}{2} \right) - k' \Theta \right] E_1^{(1)} |E_1^{(1)}|^2 - k' \Phi \frac{1}{\pi} \int_{-\infty}^{+\infty} d\xi'' \frac{|E_1^{(1)}(\xi'', \tau')|^2}{\xi' - \xi''} E_1^{(1)} = 0 \quad (\text{A72})$$

Rearranging the terms in equation gives us,

$$i \frac{\partial E_1^{(1)}}{\partial \tau'} + G \frac{\partial^2 E_1^{(1)}}{\partial \xi'^2} + q E_1^{(1)} |E_1^{(1)}|^2 + s \frac{1}{\pi} \mathcal{P} \int_{-\infty}^{+\infty} d\xi'' \frac{|E_1^{(1)}(\xi'', \tau')|^2}{\xi' - \xi''} E_1^{(1)} = 0 \quad (\text{A73})$$

where the equation is written in MFR while the coefficients are estimated in PFR. The integrals being scalars can be estimated in the PFR via Lorentz transformation from MFR. Please note the derivation was done using $c = 1$, we have reintroduced c in the appropriate places below.

This has been done by identifying c always appears as $m_\alpha c$.

$$G = \gamma_{\text{gr}}^3 \frac{1}{2} \frac{d^2 \omega}{dk^2} \quad (\text{A74})$$

$$q = -\frac{1}{2} \left(\frac{\omega - kv_{\text{gr}}}{k} \right) \left[\left(\frac{A^2}{6k} + \frac{B}{2} \right) - k \Theta \right] \quad (\text{A75})$$

$$s = \frac{\omega - kv_{\text{gr}}}{2} \Phi \quad (\text{A76})$$

$$A = \frac{1}{c} \sum_\alpha \omega_{\text{p},\alpha}^2 \int_{-\infty}^{+\infty} dp \frac{1}{(\omega - kv)} \frac{\partial}{\partial p} \left\{ \left(\frac{e_\alpha}{m_\alpha c} \right) \frac{\partial f_\alpha^{(0)}}{\partial p} \frac{1}{(\omega - kv)} \right\} \quad (\text{A77})$$

$$B = \frac{1}{c} \sum_\alpha \omega_{\text{p},\alpha}^2 \int_{-\infty}^{+\infty} dp \frac{1}{(\omega - kv)} \left(\frac{e_\alpha}{m_\alpha c} \right) \frac{\partial}{\partial p} \left[\frac{1}{(\omega - kv)} \frac{\partial}{\partial p} \left\{ \left(\frac{e_\alpha}{m_\alpha c} \right) \frac{\partial f_\alpha^{(0)}}{\partial p} \frac{1}{(\omega - kv)} \right\} \right] \quad (\text{A78})$$

$$\Theta = \left\{ \frac{H(W^2 - V^2) + 2WVU}{H^2 + U^2} + C \right\} \quad (\text{A79})$$

$$\Phi = \left\{ \frac{U(W^2 - V^2) - 2WVH}{H^2 + U^2} + D \right\} \quad (\text{A80})$$

$$C = -\frac{1}{c} \sum_\alpha \omega_{\text{p},\alpha}^2 \mathcal{P} \int_{-\infty}^{+\infty} dp \left(\frac{e_\alpha}{m_\alpha c} \right)^2 \frac{1}{(\omega - kv)^2} \frac{dv}{dv - v_{\text{gr}}} \frac{\partial}{\partial p} \left\{ \frac{(v - v_{\text{gr}})}{(\omega - kv)^2} \frac{\partial f_\alpha^{(0)}}{\partial p} \right\} \quad (\text{A81})$$

$$D = \pi \frac{1}{c} \sum_\alpha \omega_{\text{p},\alpha}^2 \int_{-\infty}^{+\infty} dp \left(\frac{e_\alpha}{m_\alpha c} \right)^2 \frac{1}{(\omega - kv)^2} \frac{dv}{dv - v_{\text{gr}}} \delta(v - v_{\text{gr}}) \frac{\partial}{\partial p} \left\{ \frac{v - v_{\text{gr}}}{(\omega - kv)^2} \frac{\partial f_\alpha^{(0)}}{\partial p} \right\} \quad (\text{A82})$$

$$W = \frac{1}{c} \sum_\alpha \omega_{\text{p},\alpha}^2 \mathcal{P} \int_{-\infty}^{+\infty} dp \frac{1}{v - v_{\text{gr}}} \frac{dv}{dv - v_{\text{gr}}} \frac{1}{(\omega - kv)^2} \left\{ \frac{e_\alpha}{m_\alpha c} \frac{\partial f_\alpha^{(0)}}{\partial p} \right\} \quad (\text{A83})$$

$$V = \pi \frac{1}{c} \sum_\alpha \omega_{\text{p},\alpha}^2 \int_{-\infty}^{+\infty} dp \delta(v - v_{\text{gr}}) \frac{dv}{dv - v_{\text{gr}}} \frac{1}{(\omega - kv)^2} \left\{ \frac{e_\alpha}{m_\alpha c} \frac{\partial f_\alpha^{(0)}}{\partial p} \right\} \quad (\text{A84})$$

$$H = \frac{1}{c} \sum_\alpha \omega_{\text{p},\alpha}^2 \mathcal{P} \int_{-\infty}^{+\infty} dp \frac{1}{v - v_{\text{gr}}} \frac{\partial f_\alpha^{(0)}}{\partial p} \quad (\text{A85})$$

$$U = \pi \frac{1}{c} \sum_\alpha \omega_{\text{p},\alpha}^2 \int_{-\infty}^{+\infty} dp \delta(v - v_{\text{gr}}) \frac{\partial f_\alpha^{(0)}}{\partial p} \quad (\text{A86})$$

Note that the expressions for the coefficients are consistent with that of MP80, PM80, MP84 and MGP00 for an electron-positron plasma. It must be mentioned here that [Ichikawa & Taniuti \(1973\)](#) used a similar scheme for deriving the NLSE in non-relativistic plasmas. However, their scheme was based on Galilean transformation and is not applicable for ultra-relativistic plasmas as is the case for pulsar plasma. It must also be mentioned that an alternative mathematical scheme could have been taken where the MFR would move with arbitrary velocity λ with respect to PFR, and both the slow space and time variables retained upto first and second order in ϵ . In that case we would obtain NLSE with additional terms. However, when λ is identified with group velocity of Langmuir waves in PFR, then the additional terms vanishes and we recover NLSE with NLD.

APPENDIX B: ESTIMATING NLSE COEFFICIENTS

The linear Langmuir dispersion relation is given by

$$k + \sum_\alpha \omega_{\text{p},\alpha}^2 \int_{-\infty}^{+\infty} dp \frac{\partial f_\alpha^{(0)}}{\partial p} \frac{1}{(\omega - kv)^2} = 0, \quad (\text{B1})$$

Differentiating the above expression with respect to the wave number k we get,

$$1 - \sum_\alpha \omega_{\text{p},\alpha}^2 \int_{-\infty}^{+\infty} dp \frac{\partial f_\alpha^{(0)}}{\partial p} \frac{1}{(\omega - kv)^2} \left[\frac{d\omega}{dk} - v \right] = 0, \quad (\text{B2})$$

where $d\omega/dk$ is the group velocity (v_{gr}) of the Langmuir waves. Rearranging the equation above we get,

$$\beta_{\text{gr}} = \frac{1}{c} \frac{d\omega}{dk} = \frac{1 + \sum_\alpha \left(\frac{\omega_{\text{p},\alpha}}{kc} \right)^2 \int_{-\infty}^{+\infty} dp \frac{\partial f_\alpha^{(0)}}{\partial p} \frac{\beta}{(\beta_{\text{ph}} - \beta)^2}}{\sum_\alpha \left(\frac{\omega_{\text{p},\alpha}}{kc} \right)^2 \int_{-\infty}^{+\infty} dp \frac{\partial f_\alpha^{(0)}}{\partial p} \frac{1}{(\beta_{\text{ph}} - \beta)^2}} \quad (\text{B3})$$

where equation (B1) can be re-expressed by performing integration by parts to give the wave number kc as,

$$k^2 c^2 = \sum_{\alpha} \omega_{p,\alpha}^2 \int_{-\infty}^{+\infty} dp f_{\alpha}^{(0)} \frac{1}{\gamma^3 (\beta_{ph} - \beta)^2}, \quad (\text{B4})$$

The momentum pole corresponding to the group velocity is given by

$$p_{gr} = \gamma_{gr} \beta_{gr} = \frac{\beta_{gr}}{\sqrt{1 - \beta_{gr}^2}}, \quad (\text{B5})$$

B1 Classification of integrals

All the integrals are written in the plasma frame of reference (PFR).

The integrals of the NLSE can be divided into three classes (as shown in Table B2)

- Regular integrals with no poles
- Interpolation of delta-function integrals at the group velocity pole
- Principal value integrals with group velocity pole

The integrals can again be sub-divided into the following categories

- Charge-dependent on the plasma particle species
- Charge independent of the plasma particle species

The integrals can be represented into their dimensionless as shown in Table B3. Using the dimensionless form of the integrals, the coefficients of NLSE (G, q, s) can also be represented in their dimensionless form as shown below.

The group velocity dispersion term G is given by

$$G = \gamma_0^3 \frac{1}{2} \frac{d^2 \omega}{dk^2} = \frac{c^2}{\omega_p} G_d \quad (\text{B6})$$

where

$$G_d = \frac{1}{2} \gamma_0^3 \left\{ (\beta_{gr} - \beta_{ph}) \left(\frac{\omega_p}{kc} \right)^3 \sum_{\alpha} \chi_{\alpha} \varphi_{\alpha} \int_{-\infty}^{+\infty} dp \frac{\partial f_{\alpha}^{(0)}}{\partial p} \frac{(\beta_{gr} - \beta)^2}{(\beta_{ph} - \beta)^3} \right\} \quad (\text{B7})$$

The non-linear co-efficient q is given by

$$q = \frac{1}{\omega_p} \left(\frac{e}{m_e c} \right)^2 q_d, \quad (\text{B8})$$

where

$$q_d = -\frac{1}{2} (\beta_{ph} - \beta_{gr}) \left\{ \left[\left(\frac{\omega_p}{kc} \right) \frac{A_d^2}{6} + \mathbf{B}_d \right] - \left(\frac{kc}{\omega_p} \right) \Theta_d \right\} \quad (\text{B9})$$

$$\Theta_d = \frac{H_d (W_d^2 - V_d^2) + 2W_d V_d U_d}{H_d^2 + U_d^2} + C_d \quad (\text{B10})$$

The non-linear Landau damping co-efficient s is given by

$$s = \frac{1}{\omega_p} \left(\frac{e}{m_e c} \right)^2 s_d, \quad (\text{B11})$$

where

$$s_d = \frac{1}{2} (\beta_{ph} - \beta_{gr}) \left(\frac{kc}{\omega_p} \right) \Phi_d \quad (\text{B12})$$

$$\Phi_d = \frac{U_d (W_d^2 - V_d^2) - 2W_d V_d H_d}{H_d^2 + U_d^2} + D_d \quad (\text{B13})$$

From equation (B8) and equation (B11) we have,

$$\frac{s}{q} = \frac{s_d}{q_d} = - \frac{\left(\frac{kc}{\omega_p}\right) \Phi_d}{\left[\left(\frac{\omega_p}{kc}\right) \frac{A_d^2}{6} + B_d\right] - \left(\frac{kc}{\omega_p}\right) \Theta_d}, \quad (\text{B14})$$

It must be noted that the group velocity v_{gr} contribution to s/q is due to Φ_d and Θ_d (see Table B2).

B2 Computing Cauchy Principal Integral due to group velocity pole

The integrals for the co-efficients of NLSE expressed as equation (3) are a function of the particle distribution functions, the number density of the plasma particles and the linear wave dispersion relation of the subluminal Langmuir waves (ω, k) in PFR. The v and v_{gr} represent the velocity of the plasma particles and the group velocity (v_{gr}) of the group velocity of linear Langmuir waves respectively. The integrals which two Cherenkov terms viz., a phase velocity Cherenkov term ($\omega - kv$) and the group velocity Cherenkov term ($\omega - kv_{gr}$). In our present study, we assume that the phase velocity of the linear Langmuir waves exceeds the particle velocities ($\omega/k > v$) such that the only pole in the integrals is due to group velocity ($v_{gr} = d\omega/dk$) of the linear Langmuir waves. To ensure this the momentum corresponding to wave phase velocity (p_{ph}) must be taken much farther from the mean momenta (p_α) of the particle distribution function of the α -th species. The wave phase velocity (notmalized to c) is $\beta_{ph} = p_{ph}/\sqrt{1^2 + p_{ph}^2}$.

Consider a function $f(p)$ with a pole at $p = p_{gr}$. Consider the Cauchy Principal Value Integral of $f(p)$ given by

$$\begin{aligned} I &= \mathcal{P} \int_{p_l}^{p_h} dp f(p) \\ &= \lim_{\epsilon \rightarrow 0} \left[\int_{p_l}^{p_{gr}-\epsilon} dp f(p) + \text{Re}(I_0) + \int_{p_{gr}+\epsilon}^{p_h} dp f(p) \right] \\ &= I_- + I_{\text{pole}} + I_+ \end{aligned} \quad (\text{B15})$$

Next we consider a semi-circular contour centred at p_{gr} and of radius ϵ in the complex \tilde{p} plane

$$\begin{aligned} \tilde{p} &= p_{gr} + \epsilon \exp(i\theta) \\ d\tilde{p} &= i\epsilon \exp(i\theta) d\theta \end{aligned}$$

Then we have the integral

$$I_0 = \oint_{p_{gr}-\epsilon}^{p_{gr}+\epsilon} d\tilde{p} f(\tilde{p}) = i\epsilon \int_{\theta=\pi}^{\theta=0} d\theta e^{i\theta} f(p_{gr} + \epsilon e^{i\theta})$$

Finally we have

$$\begin{aligned} I_{\text{pole}} &= \text{Re} \left[\lim_{\epsilon \rightarrow 0} I_0 \right] \\ &= \text{Re} \left[\lim_{\epsilon \rightarrow 0} i\epsilon \int_{\theta=\pi}^{\theta=0} d\theta e^{i\theta} f(p_{gr} + \epsilon e^{i\theta}) \right] \end{aligned}$$

B3 Introduction of α -th species

We introduce the following notation

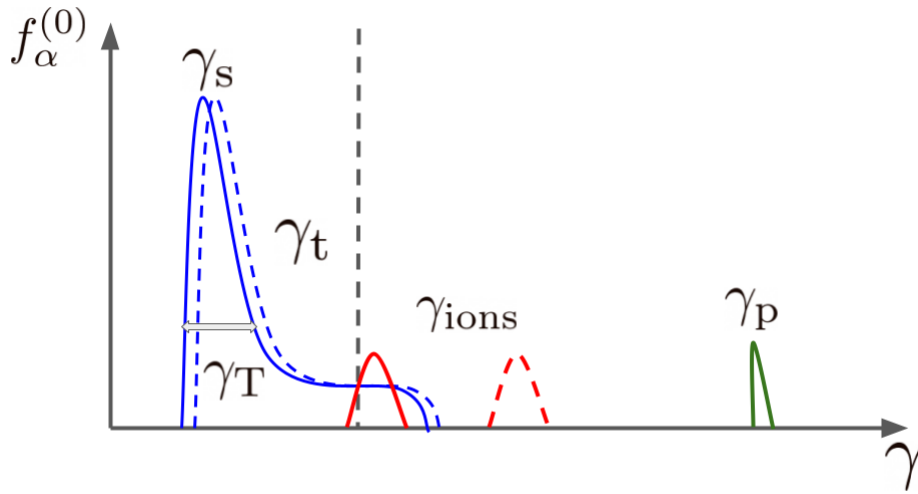
$$\varphi_\alpha = Z_\alpha \times \frac{m_e}{m_\alpha}, \quad (\text{B16})$$

$$\chi_\alpha = \frac{Z_\alpha}{A_\alpha} \times \frac{n_\alpha}{n_p}, \quad (\text{B17})$$

$$\frac{\omega_{p,\alpha}^2}{\omega_p^2} = \chi_\alpha \varphi_\alpha, \quad (\text{B18})$$

Table B1. For α -th species in the plasma, φ_α is the ratio of charge to mass in units of (e/m_e) and χ_α is the ratio of number density of the plasma to the number density of pair plasma. The subscript \pm stands for positrons and electrons in the pair plasma respectively. The subscript ion stands for the ion contribution.

Quantity	Value
φ_+	1
φ_-	1
φ_{ion}	1.42×10^{-2}
χ_+	1
χ_-	1
χ_{ion}	10^{-4}



[h]

Figure B1. A schematic of the particle distribution function and the pole of the group velocity (shown as horizontal dashed line). Only particles in the immediate neighbourhood of the pole due to group velocity can contribute to resonant interaction that characterizes the dimensionless coefficients s_d and q_d respectively. The electron and positron DF of the pair plasma is shown in solid blue and dashed line respectively. The DF of the positron beam (shown in solid green) is far-removed from the pole. The DF due to iron can contribute only if located near the pole (as shown in solid red) and will fail do so if away from the pole (as shown in dashed red). It must be noted that the peaks of the electron and positron DF are separated due to plasma outflow along curved magnetic field lines as shown in Appendix F.

where

$$Z_\alpha = \left| \frac{e_\alpha}{e} \right|, \quad (\text{B19})$$

$$\omega_p^2 = \frac{4\pi n_s e^2}{m_e}, \quad (\text{B20})$$

For ions we have,

$$\omega_{\text{ion}}^2 = \left\{ \frac{Z_{\text{ion}}^2}{A_{\text{ion}}} \times \frac{m_e}{m_p} \times \frac{n_{\text{ion}}}{n_s} \right\} \omega_p^2 = \varphi_{\text{ion}} \chi_{\text{ion}} \omega_p^2, \quad (\text{B21})$$

For iron ions we have,

$$\begin{aligned} Z_{\text{ion}} &= 26 \\ A_{\text{ion}} &= 56 \\ \frac{m_p}{m_e} &= 1836 \\ \frac{n_{\text{ion}}}{n_s} &= \frac{1}{\kappa} \approx 10^{-4} \end{aligned}$$

Typical estimates for quantities defined in equation (B16) and equation (B17) are presented in Table B1.

Table B2. Classification of integrals for the coefficients in NLSE. The contribution of the group velocity v_{gr} in the Interpolation and the Principal value integrals must be noted.

Type	Charge-dependence	Integral
Regular	Yes	$A = \frac{1}{c} \sum_{\alpha} \omega_{\text{p},\alpha}^2 \int_{-\infty}^{+\infty} dp \frac{1}{(\omega-kv)} \frac{\partial}{\partial p} \left\{ \left(\frac{e_{\alpha}}{m_{\alpha}c} \right) \frac{\partial f_{\alpha}^{(0)}}{\partial p} \frac{1}{(\omega-kv)} \right\}$
	No	$B = \frac{1}{c} \sum_{\alpha} \omega_{\text{p},\alpha}^2 \int_{-\infty}^{+\infty} dp \frac{1}{(\omega-kv)} \frac{\partial}{\partial p} \left\{ \left(\frac{e_{\alpha}}{m_{\alpha}c} \right) \frac{1}{(\omega-kv)} \frac{\partial}{\partial p} \left\{ \left(\frac{e_{\alpha}}{m_{\alpha}c} \right) \frac{\partial f_{\alpha}^{(0)}}{\partial p} \frac{1}{(\omega-kv)} \right\} \right\}$
Interpolation	Yes	$V = \pi \frac{1}{c} \sum_{\alpha} \omega_{\text{p},\alpha}^2 \int_{-\infty}^{+\infty} dp \delta(v - v_{\text{gr}}) \frac{dv}{dp} \frac{1}{(\omega-kv)^2} \left\{ \left(\frac{e_{\alpha}}{m_{\alpha}c} \right) \frac{\partial f_{\alpha}^{(0)}}{\partial p} \right\}$
	No	$D = \pi \frac{1}{c} \sum_{\alpha} \omega_{\text{p},\alpha}^2 \int_{-\infty}^{+\infty} dp \left(\frac{e_{\alpha}}{m_{\alpha}c} \right)^2 \frac{1}{(\omega-kv)^2} \frac{dv}{dp} \delta(v - v_{\text{gr}}) \frac{\partial}{\partial p} \left\{ \frac{(v-v_{\text{gr}})}{(\omega-kv)^2} \frac{\partial f_{\alpha}^{(0)}}{\partial p} \right\}$
	No	$U = \pi \frac{1}{c} \sum_{\alpha} \omega_{\text{p},\alpha}^2 \int_{-\infty}^{+\infty} dp \delta(v - v_{\text{gr}}) \frac{\partial f_{\alpha}^{(0)}}{\partial p}$
Principal value	Yes	$W = \frac{1}{c} \sum_{\alpha} \omega_{\text{p},\alpha}^2 \mathcal{P} \int_{-\infty}^{+\infty} dp \frac{1}{(v-v_{\text{gr}})} \frac{dv}{dp} \frac{1}{(\omega-kv)^2} \left\{ \left(\frac{e_{\alpha}}{m_{\alpha}c} \right) \frac{\partial f_{\alpha}^{(0)}}{\partial p} \right\}$
	No	$C = -\frac{1}{c} \sum_{\alpha} \omega_{\text{p},\alpha}^2 \mathcal{P} \int_{-\infty}^{+\infty} dp \left(\frac{e_{\alpha}}{m_{\alpha}c} \right)^2 \frac{1}{(\omega-kv)^2} \frac{dv}{dp} \frac{1}{(v-v_{\text{gr}})} \frac{\partial}{\partial p} \left\{ \frac{(v-v_{\text{gr}})}{(\omega-kv)^2} \frac{\partial f_{\alpha}^{(0)}}{\partial p} \right\}$
	No	$H = \frac{1}{c} \sum_{\alpha} \omega_{\text{p},\alpha}^2 \mathcal{P} \int_{-\infty}^{+\infty} dp \frac{1}{(v-v_{\text{gr}})} \frac{\partial f_{\alpha}^{(0)}}{\partial p}$

B4 Setup for maximizing the contributions due to ions

The integrals as shown in Table B2 depend on the derivative of the particle distribution function around the group velocity pole as shown in Fig. B1. Ions have a unique advantage in that location of the ion distribution function is close to the electron and positron distribution function. In order to maximise the contribution of an ion distribution function to the integrals presented in Table B3, the peak of the ion distribution function (\bar{p}_{ion}) (for both Lorentzian and Gaussian distribution function) is chosen to be at

$$\bar{p}_{\alpha} = \sigma \pm p_{\text{gr}}, \quad \text{For Gaussian DF} \quad (\text{B22})$$

$$\bar{p}_{\alpha} = \Delta p \pm p_{\text{gr}}, \quad \text{For Lorentzian DF} \quad (\text{B23})$$

so to maximize the derivative of the ion distribution function at p_{gr} .

We find that the contribution of ions in modifying the dimensionless coefficients is very small ($\delta G_{\text{d}}, \delta s_{\text{d}}, \delta q_{\text{d}} \leq 10^{-8}$).

APPENDIX C: PARAMETERS FOR THE NUMERICAL SIMULATION

To solve NLSE with NLD numerically we use the integrating factor and Leap frog method (IF-LF) numerical method as Lakoba (2017) and Lakoba et al. (2018).

While an expanded discussion is already available in the previously mentioned works, some essential steps are reproduced below for the sake of completion.

The dimensionless non-linear Schrodinger equation (NLSE) with non-linear Landau damping (NLD) term is

$$i \frac{\partial u}{\partial t} + \frac{\partial^2 u}{\partial x^2} + Qu \left(|u|^2 + \frac{s}{\pi q} \mathcal{P} \int_{-\infty}^{+\infty} dx' \frac{|u(x', t)|^2}{x - x'} \right) = 0 \quad (\text{C1})$$

We define

$$\hat{u}(k, t) = \frac{1}{\sqrt{2\pi}} \int_{-\infty}^{+\infty} dx u(x, t) e^{-ikx} \quad (\text{C2})$$

such that

$$u(x, t) = \frac{1}{\sqrt{2\pi}} \int_{-\infty}^{+\infty} dx \hat{u}(k, t) e^{ikx} \quad (\text{C3})$$

Table B3. Conversion of the integrals from dimensional form to dimensionless form. The quantities β_{ph} , β_{gr} and β are wave phase velocity, wave group velocity and particle velocity normalised to the speed of light c . The quantities φ_α and χ_α are defined in equation (B16) and equation (B17) respectively. In the charge dependent integrals the quantity sign_α is +1 for positrons and ions and -1 for electrons.

Dimensional	Dimensionless
$A = \frac{1}{c} \left(\frac{ e }{m_e c} \right) \sum_\alpha A_{d,\alpha} = \frac{1}{c} \left(\frac{ e }{m_e c} \right) A_d$	$A_{d,\alpha} = \left(\frac{\omega_p}{kc} \right)^2 \text{sign}_\alpha \varphi_\alpha^2 \chi_\alpha \int_{-\infty}^{+\infty} dp \frac{1}{(\beta_{\text{ph}} - \beta)} \frac{\partial}{\partial p} \left\{ \frac{\partial f_\alpha^{(0)}}{\partial p} \frac{1}{(\beta_{\text{ph}} - \beta)} \right\}$
$B = \frac{1}{c} \left(\frac{e}{m_e c} \right)^2 \frac{1}{\omega_p} \sum_\alpha B_{d,\alpha} = \frac{1}{c} \left(\frac{e}{m_e c} \right)^2 \frac{1}{\omega_p} B_d$	$B_{d,\alpha} = \left(\frac{\omega_p}{kc} \right)^3 \varphi_\alpha^3 \chi_\alpha \int_{-\infty}^{+\infty} dp \frac{1}{(\beta_{\text{ph}} - \beta)} \frac{\partial}{\partial p} \left[\frac{1}{(\beta_{\text{ph}} - \beta)} \frac{\partial}{\partial p} \left\{ \frac{\partial f_\alpha^{(0)}}{\partial p} \frac{1}{(\beta_{\text{ph}} - \beta)} \right\} \right]$
$V = \frac{1}{c} \left(\frac{ e }{m_e c} \right) \sum_\alpha V_{d,\alpha} = \frac{1}{c} \left(\frac{ e }{m_e c} \right) V_d$	$V_{d,\alpha} = \pi \left(\frac{\omega_p}{kc} \right)^2 \text{sign}_\alpha \varphi_\alpha^2 \chi_\alpha \int_{-\infty}^{+\infty} dp \delta(p - p_{\text{gr}}) \frac{1}{(\beta_{\text{ph}} - \beta)^2} \frac{\partial f_\alpha^{(0)}}{\partial p}$
$D = \left(\frac{e}{m_e c} \right)^2 \frac{1}{\omega_p^2} \sum_\alpha D_{d,\alpha} = \left(\frac{e}{m_e c} \right)^2 \frac{1}{\omega_p^2} D_d$	$D_{d,\alpha} = \pi \left(\frac{\omega_p}{kc} \right)^4 \varphi_\alpha^3 \chi_\alpha \int_{-\infty}^{+\infty} dp \frac{1}{(\beta_{\text{ph}} - \beta)^2} \delta(p - p_{\text{gr}}) \frac{\partial}{\partial p} \left\{ \frac{\partial f_\alpha^{(0)}}{\partial p} \frac{\beta - \beta_{\text{gr}}}{(\beta_{\text{ph}} - \beta)^2} \right\}$
$U = \frac{\omega_p^2}{c^2} \sum_\alpha U_{d,\alpha} = \frac{\omega_p^2}{c^2} U_d$	$U_{d,\alpha} = \pi \varphi_\alpha \chi_\alpha \int_{-\infty}^{+\infty} dp \gamma^3 \delta(p - p_{\text{gr}}) \frac{\partial f_\alpha^{(0)}}{\partial p}$
$W = \frac{1}{c} \left(\frac{ e }{m_e c} \right) \sum_\alpha W_{d,\alpha} = \frac{1}{c} \left(\frac{ e }{m_e c} \right) W_d$	$W_{d,\alpha} = \left(\frac{\omega_p}{kc} \right)^2 \text{sign}_\alpha \varphi_\alpha^2 \chi_\alpha \mathcal{P} \int_{-\infty}^{+\infty} dp \frac{1}{(\beta - \beta_{\text{gr}})} \frac{1}{\gamma^3} \frac{1}{(\beta_{\text{ph}} - \beta)^2} \frac{\partial f_\alpha^{(0)}}{\partial p}$
$C = \left(\frac{e}{m_e c} \right)^2 \frac{1}{\omega_p^2} \sum_\alpha C_{d,\alpha} = \left(\frac{e}{m_e c} \right)^2 \frac{1}{\omega_p^2} C_d$	$C_{d,\alpha} = - \left(\frac{\omega_p}{kc} \right)^4 \varphi_\alpha^3 \chi_\alpha \mathcal{P} \int_{-\infty}^{+\infty} dp \frac{1}{(\beta_{\text{ph}} - \beta)^2} \frac{1}{\gamma^3} \frac{1}{(\beta - \beta_{\text{gr}})} \frac{\partial}{\partial p} \left\{ \frac{(\beta - \beta_{\text{gr}})}{(\beta_{\text{ph}} - \beta)^2} \frac{\partial f_\alpha^{(0)}}{\partial p} \right\}$
$H = \frac{\omega_p^2}{c^2} \sum_\alpha H_{d,\alpha} = \frac{\omega_p^2}{c^2} H_d$	$H_{d,\alpha} = \varphi_\alpha \chi_\alpha \mathcal{P} \int_{-\infty}^{+\infty} dp \frac{1}{(\beta - \beta_{\text{gr}})} \frac{\partial f_\alpha^{(0)}}{\partial p}$

We can reduce equation (C1) to the form

$$i u_t + \mathcal{L} u + \mathcal{N} = 0 \quad (\text{C4})$$

where

$$\mathcal{L} = \frac{\partial^2}{\partial x^2} \quad (\text{C5})$$

$$\mathcal{N} = Q u \left(|u|^2 + \frac{s}{\pi q} \mathcal{P} \int_{-\infty}^{+\infty} dx' \frac{|u(x', t)|^2}{x - x'} \right) \quad (\text{C6})$$

Taking Fourier transform **FT** of equation (C4) we get,

$$i \hat{u}_t + \hat{\mathcal{L}} \hat{u} + \hat{\mathcal{N}} = 0 \quad (\text{C7})$$

where $\hat{\mathcal{L}} = -k^2$.

Solution of equation (C7) from time t_2 to time t_1 has the form

$$e^{-i \hat{\mathcal{L}} t_2} \hat{u}(t_2) - e^{-i \hat{\mathcal{L}} t_1} \hat{u}(t_1) = \int_{t_1}^{t_2} e^{-i \hat{\mathcal{L}} t'} i \hat{\mathcal{N}}(t') dt' \quad (\text{C8})$$

where

$$\hat{\mathcal{N}}(k, t) = \mathbf{FT}[(Q|u|^2 + V(x))u] \quad (\text{C9})$$

$$V(x) = \chi Q \frac{1}{2\pi} \int_{-\infty}^{+\infty} dk e^{ikx} \left[\frac{i}{\sqrt{2\pi}} \text{sgn}(k) \times \int_{-\infty}^{+\infty} dx e^{-ikx} |u|^2 \right] = \frac{\chi Q}{2} \mathcal{H}[|u|^2] \quad (\text{C10})$$

where the the Hilbert transform \mathcal{H} of $|u|^2$ is defined as

$$\mathcal{H}[|u(x, t)|^2] = \frac{1}{\pi} \mathcal{P} \int_{-\infty}^{+\infty} dx' \frac{|u(x', t)|^2}{x - x'} = \frac{1}{\pi} \lim_{\epsilon \rightarrow 0^+} \left(\int_{x-1/\epsilon}^{x-\epsilon} dx' \frac{|u(x', t)|^2}{x - x'} + \int_{x+\epsilon}^{x+1/\epsilon} \frac{|u(x', t)|^2}{x - x'} \right) \quad (\text{C11})$$

Next, we employ the three-point numerical scheme where

$$t' = t_n = n \Delta t \quad (\text{C12})$$

$$t_2 = t_{n+1} = (n+1) \Delta t \quad (\text{C13})$$

$$t_1 = t_{n-1} = (n-1) \Delta t \quad (\text{C14})$$

□

Table C1. Parameters of the box used for simulation. The quantity L denotes the length of the simulation box, the quantity N denotes, the number of grid-points, the highest wave number k_{\max} in the Fourier domain, the quantity $\Delta t_{\text{crit}} = \pi/k_{\max}^2$ is the time interval above which parasitic solutions leads to rapid saturation of power at higher harmonics and $\Delta t < \Delta t_{\text{crit}}$ is the time interval used for the simulation, t_{\max} is the maximum run time of the simulation and Th_{300} is value of $\log_{10}(F[u])$ at $k = 300$ beyond which the simulation is stopped.

L	N	k_{\max}	Δt_{crit}	Δt	t_{\max}	Th_{300}
40π	12288	308	3e-5	1e-5	100	1e-2

The application of the 3-point numerical scheme reduces equation (C8) to the form

$$e^{ik^2\Delta t} \hat{u}(t_{n+1}) - e^{-ik^2\Delta t} \hat{u}(t_{n-1}) = 2i \Delta t \hat{\mathcal{N}}(t_n) \quad (\text{C15})$$

Next we define,

$$\hat{v}_n = \hat{u}_n e^{ik^2 t_n} = \hat{u}_n e^{ik^2 n\Delta t} \quad (\text{C16})$$

Substituting equation (C16) in equation (C15) we get

$$\hat{v}_{n+1} - \hat{v}_{n-1} = 2i \Delta t e^{ik^2 t_n} \hat{\mathcal{N}}(t_n) \quad (\text{C17})$$

For checking numerical stability we need to evaluate the following quantities after every eight time steps

$$\hat{v}_n = a_0 \hat{v}_n + a_1 (\hat{v}_{n-1} + \hat{v}_{n+1}) + a_2 (\hat{v}_{n-2} + \hat{v}_{n+2}) + a_3 (\hat{v}_{n-3} + \hat{v}_{n+3}) \quad (\text{C18})$$

$$\hat{v}_{n-1} = a_0 \hat{v}_{n-1} + a_1 (\hat{v}_{n-2} + \hat{v}_n) + a_2 (\hat{v}_{n-3} + \hat{v}_{n+1}) + a_3 (\hat{v}_{n-4} + \hat{v}_{n+2}) \quad (\text{C19})$$

where $a_0 = \frac{11}{16}$; $a_1 = \frac{15}{64}$; $a_2 = -\frac{3}{32}$; $a_3 = \frac{1}{64}$.

After every eight time steps, we use \hat{v}_n and \hat{v}_{n-1} to restart equation (C16) by replacing, on the l.h.s., \hat{v}_{n-1} with \hat{v}_{n-1} and, on the r.h.s., \hat{v}_n with \hat{v}_{n-1} . As shown in Lakoba (2017) this procedure suppresses the parasitic solution at the edges of the spectral window for long time of evolution and requires that the interval Δt to be smaller than a critical time interval given by

$$\Delta t < \Delta t_{\text{crit}} = \frac{\pi}{k_{\max}^2}, \quad (\text{C20})$$

In what follows we briefly describe the simulation box parameters. For a box of length L (normalised to θ) with N grid points, the spacing interval is given by

$$\Delta x = \frac{L}{N}, \quad (\text{C21})$$

The spacing in the Fourier domain is given by

$$dk = \frac{2\pi}{L}, \quad (\text{C22})$$

The highest value of wave number in the Fourier domain is given by

$$k_{\max} = \frac{2\pi}{2\Delta x} = \frac{\pi N}{L} \quad (\text{C23})$$

In the IF-LF method, the parasitic solutions are suppressed by choosing the discrete time interval Δt to be smaller than a critical time interval given by

$$\Delta t_{\text{crit}} = \frac{\pi}{k_{\max}^2}, \quad (\text{C24})$$

in order to suppress parasitic solution.

The simulation is terminated if the power ($\log_{10} |F(u)|$) at $k_{\max} \approx 300$ exceeds a threshold value (10^{-2}). For the numerical simulations in the main text, the simulation parameters are summarized in Table (C1).

APPENDIX D: IMPACT OF THE INITIAL INJECTED SPECTRUM ON SOLITON FORMATION

First we choose a random number generators for the white noise field $w(k)$ as defined in Eq. (24) and Eq. (25) of the main text. Then, for each of the random number generator, the simulation runs till the secondary peak in the Fourier space reaches $k = -100$. The final amplitude of $|u|$ is then measured in the configuration space. For well-formed solitons, we put the criterion that the amplitude of the soliton $|u|$ must be three

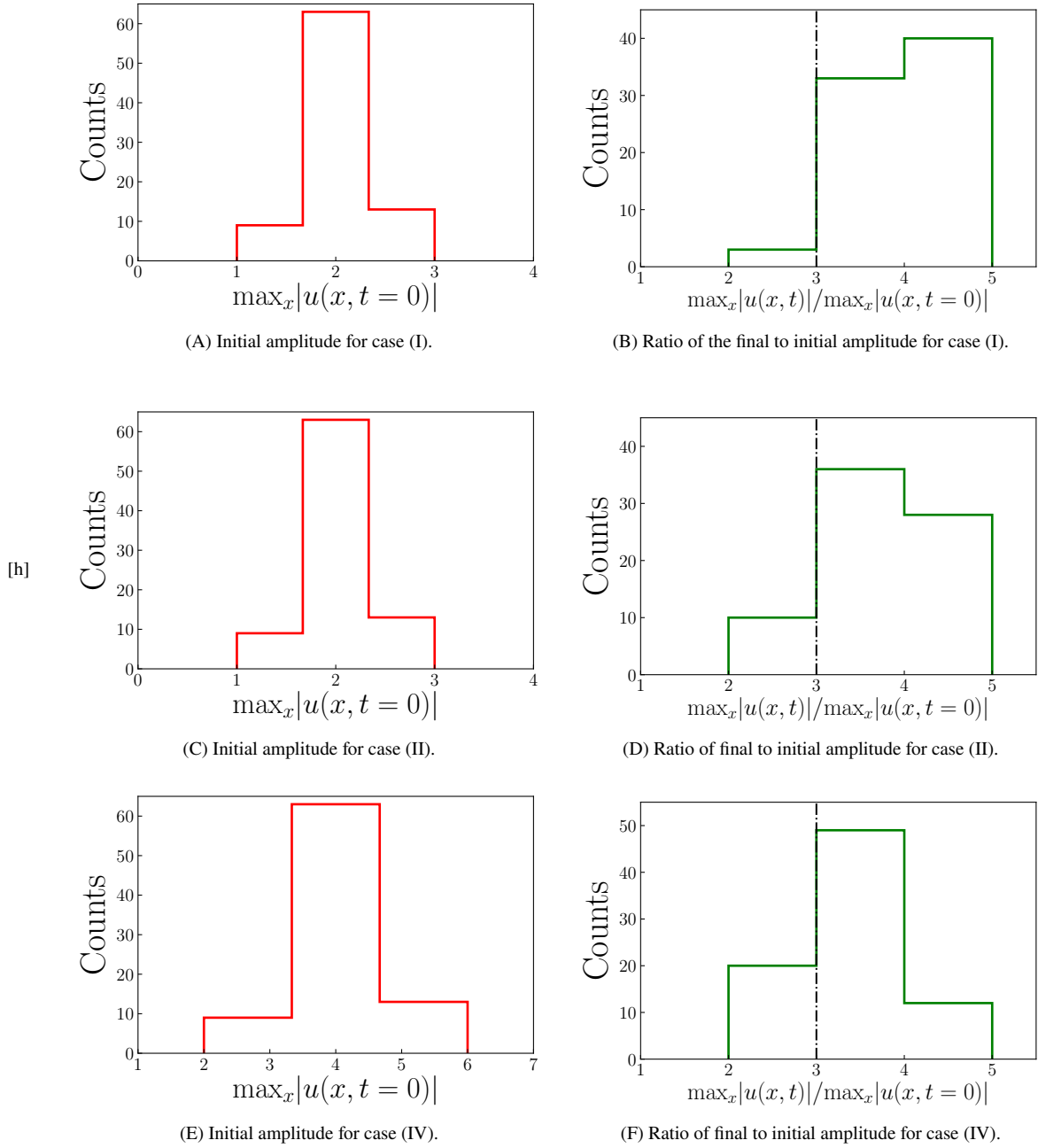


Figure D1. The histograms for the cases (I) to (III) (see D) for details. The vertical black dashed lines on all the right panels represents the threshold of 3.

times or higher than the amplitude of the initial field. We construct two histograms. The first histogram shows the amplitude of the initial field. The second histogram shows the ratio between the final amplitude and the initial amplitude. The histograms are shown in Fig. D1.

- Case I: In the first simulation we have $Q = 0.25$, $s/q = 0.1$, $k_{\text{corr}} = 2$. In this case the final amplitude of the field does exceed the initial value by 3 times.
- Case II: In the first simulation we have $Q = 0.25$, $s/q = 0.1$, $k_{\text{corr}} = 1$. We take hundred random number generators and show that the for most random number generators the final amplitude of the field does exceed the initial value by 3 times.
- Case III: In the first simulation we have $Q = 0.25$, $s/q = 0.1$, $k_{\text{corr}} = 2$, initial amplitude doubled compared to Case I.

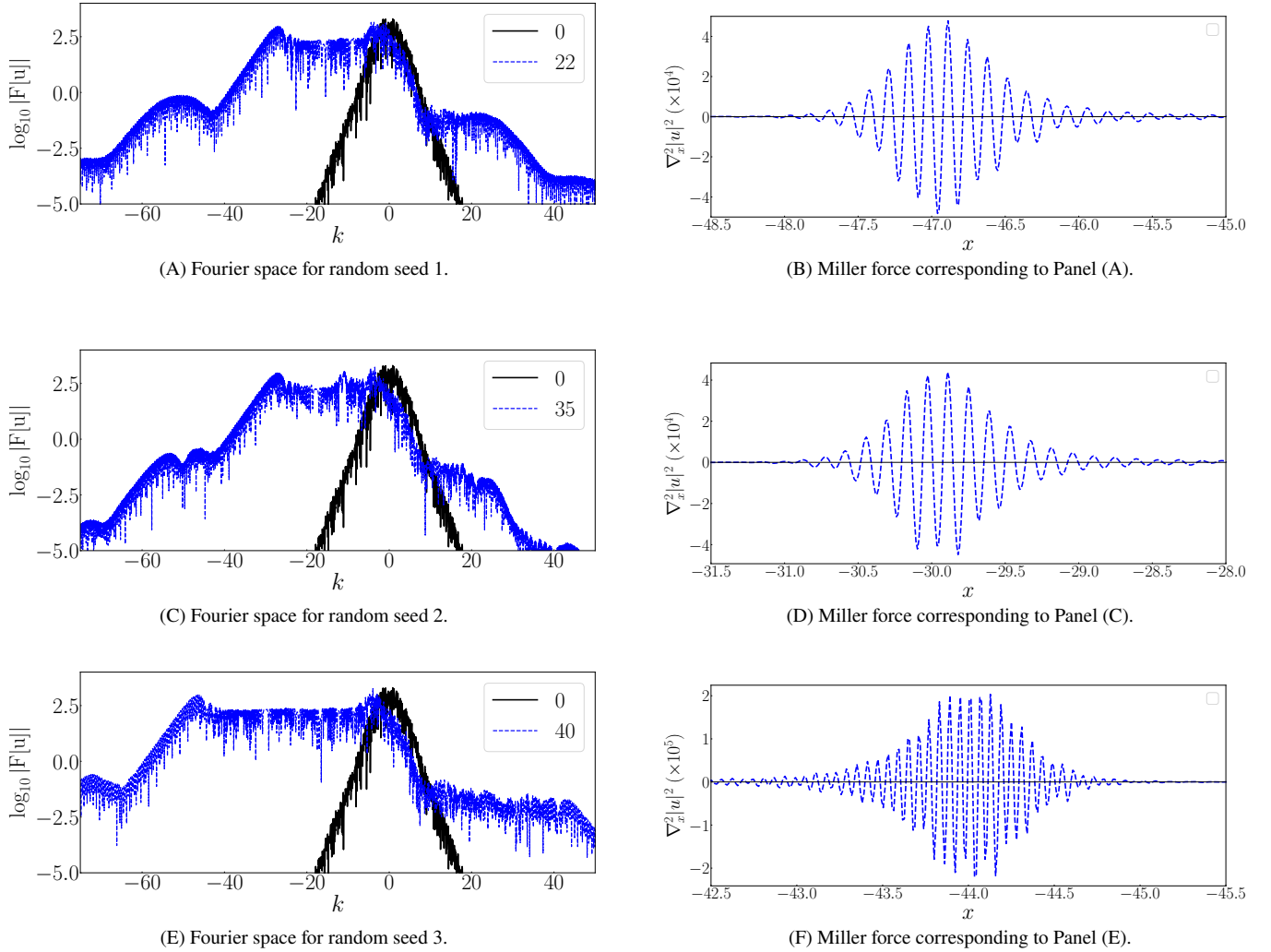


Figure E1. The figure shows the Fourier space and the configuration space for fixed ($Q = 0.25, s/q = 0.1, k_{\text{cor}} = 2$) for 3 different random seed values at times (shown in legends on the left panel) when the amplitude of the solitons exceeds the initial field amplitude by at least three times. It is seen that while the length of the soliton nearly remains constant, the number of ripples in the soliton structure is more if the secondary peak is located at a higher k . The number of ripples are similar if the secondary peak is located at similar k .

APPENDIX E: ON THE VARIATION OF RIPPLE SIZES IN SOLITONS

The criterion that we have used for a well-formed solitons is that the amplitude of the soliton must be at least three times higher than the amplitude of the initial field strength. In Fig. E1 we show that for a fixed ($Q = 0.25, s/q = 0.1, k_{\text{cor}} = 2$) we show the location of the secondary peak in the Fourier space (shown on left panels) and the Miller force (on the right panels) for three different random seed values. The time of soliton formation is indicated on the legends of the left panels. It can be seen that when the location of the secondary peak is similar (Panels(A) and (C)), the number of ripples in the Miller force is similar. As shown in Panel (E) if the peak is located at a higher k then as shown in Panel (F) the number of ripples also increases. It can be seen that the number of ripples can change as much as 50%. This variation has implications for the coherent curvature radiation pattern which will be explored in an upcoming work.

APPENDIX F: SEPARATION OF DISTRIBUTION FUNCTIONS IN CURVED MAGNETIC FIELD LINES

The following mechanism was proposed by Cheng & Ruderman (1977) (hereafter CR77). Let $\vec{\Omega}_{\text{Rot}}$ be the angular velocity of the pulsar and \vec{B} be the local magnetic field at any distance r on a given magnetic field line. The condition for the pulsar magnetosphere to co-rotate with the pulsar requires charge particles to maintain the co-rotational Goldreich-Julian value $\rho_{\text{GJ}} = \vec{\Omega}_{\text{Rot}} \cdot \vec{B} f / (2\pi c)$. Along the open magnetic field lines ρ_{GJ} is provided by the one-dimensional flow of the charged high energy beams and the quasi-neutral plasma pair plasma. Magnetically

induced pair creation cascades gets quenched at a distance of around $r_O = 1.02 R_{NS}$. Beyond r_O , no new particles are created. This implies that the total current across any cross-section of the flux tube formed by the open field lines remains constant beyond r_O . At r_O , the charged beams contribute exclusively to ρ_{GJ} . The number density of the particles decreases as the strength of the field ($\propto 1/r^3$) while Goldreich-Julian value varies as $\rho_{GJ} \propto \cos \alpha / r^3$ where α is the angle between \vec{B} and $\vec{\Omega}_{Rot}$. For the curved open field lines α changes further away from the neutron star. The divergence less nature of the current flow for $r \geq R_O$ insures that the charged beams cannot completely provide for ρ_{GJ} all along a curved field line. The pair plasma provides the offset charge density ($\delta\rho = \rho_{GJ} - \rho_b$) by acquiring a net charge density. It requires the separation of the bulk velocities of electrons and positrons in the pair plasma. We re-derive the expression for bulk-separation from CR77.

In the steady-state for which $\vec{E} \cdot \vec{B} = 0$, the charge density at any point is given by Goldreich-Julian charge density

$$\rho_{GJ} = -\frac{\vec{\Omega}_{Rot} \cdot \vec{B} f}{2\pi c} \quad (F1)$$

where

$$f = 1 + \mathcal{O}\left(\frac{\Omega_{Rot}^2 r^2}{c^2}\right)$$

is the contribution due to rotation.

The contribution to the total charge density is a summation of charge density due to each species ' α '-th such that

$$\rho_{GJ} = \sum_{\alpha} \rho_{\alpha}$$

At any arbitrary point the species present are beam (positrons, ions or both), and electrons and positrons of pair plasma such that

$$\rho_{GJ} = \rho_b + \rho_- + \rho_+ \quad (F2)$$

At the injection point 'O' the entire contribution comes from the beam such that using F1 and F2 we get

$$\rho_{GJ,O} = \rho_{b,O} = -\frac{(\vec{\Omega}_{Rot} \cdot \vec{B} f)_O}{2\pi} \quad (F3)$$

The current density at any point (\vec{r}) is given by

$$\vec{J} = \rho_{GJ} (\vec{\Omega}_{Rot} \times \vec{r}) + \vec{J}_{\parallel}$$

where \vec{J}_{\parallel} is the current in the direction of the local magnetic field \vec{B} such that

$$\vec{J}_{\parallel} = \sum_{\alpha} \vec{v}_{\parallel,\alpha} \rho_{\alpha} = \sum_{\alpha} \vec{J}_{\parallel,\alpha} \quad (F4)$$

In some portion of the field line where there is no source term (meaning there is no particle production and dissipation) we can write

$$\nabla \cdot \vec{J}_{\parallel,\alpha} = 0$$

for each component.

The solution of the above equation is given by

$$\vec{J}_{\parallel,\alpha} = -\frac{\Phi_{\alpha} \Omega_{Rot}}{2\pi} \vec{B} \quad (F5)$$

such that $\Phi_{\alpha} \Omega_{Rot}$ is an invariant along any given field line.

Using equation F4 and F5 we get

$$\vec{J}_{\parallel,b} = \rho_b c \hat{B} = -\frac{\Phi_b \Omega_{Rot}}{2\pi} \vec{B}$$

$$\vec{J}_{\parallel,\pm} = \rho_{\pm} v_{\pm} \hat{B} = -\frac{\Phi_{\pm} \Omega_{Rot}}{2\pi} \vec{B} \quad (F6)$$

where the ultra-relativistic nature of the beam particles ($v \sim c$) has been taken account.

At point 'O' using Eq F3 and F6 we get

$$\rho_{b,O} = -\frac{(\Omega_{Rot} B)_O}{2\pi c} \Phi_b = -\frac{(\vec{\Omega}_{Rot} \cdot \vec{B} f)_O}{2\pi c}$$

$$\Rightarrow \Phi_b = (\hat{\Omega}_{Rot} \cdot \hat{B} f)_O \quad (F7)$$

Similarly for e^\pm of pair plasma using equation F6 at point ‘O’ we get

$$\begin{aligned}\Phi_\pm \frac{(\Omega_{\text{Rot}} \vec{B})_O}{2\pi} &= [\rho_\pm v_\pm \hat{B}]_O \\ \Rightarrow \Phi_\pm &= -2\pi \left[\frac{\rho_\pm v_\pm}{\Omega_{\text{Rot}} B} \right]_O\end{aligned}$$

From Eq F7 we get

$$(\Omega_{\text{Rot}} B)_O = -\frac{2\pi c}{\Phi_b} \rho_{b,O} \quad (\text{F8})$$

Using this in the expression for Φ_\pm we get

$$\Phi_\pm = \left[\frac{\rho_\pm}{\rho_b} \right]_O \left[\frac{v(\pm)}{c} \right]_O \Phi_b \quad (\text{F9})$$

From Eq F1 and F2 we get for any arbitrary point ‘A’

$$1 + \frac{\rho_+}{\rho_b} + \frac{\rho_-}{\rho_b} = -\frac{\vec{\Omega}_{\text{Rot}} \cdot \vec{B} f}{2\pi c \rho_b} \quad (\text{F10})$$

Using Eq F7 and F6 we obtain

$$\rho_b = -\left(\hat{\Omega}_{\text{Rot}} \cdot \hat{B} f \right)_O \frac{\Omega_{\text{Rot}} B}{2\pi c} \quad (\text{F11})$$

Using Eq F6, F9, and F11 in Eq F10 we get

$$\begin{aligned}\frac{\rho_+}{\rho_b} + \frac{\rho_-}{\rho_b} &= \left[\frac{\hat{\Omega}_{\text{Rot}} \cdot \hat{B} f}{(\hat{\Omega}_{\text{Rot}} \cdot \hat{B} f)_O} - 1 \right] \\ \Rightarrow \frac{1}{\rho_b} \left[\Phi_+ \left(\frac{\Omega_{\text{Rot}} B}{2\pi v_+} \right) + \Phi_- \left(\frac{\Omega_{\text{Rot}} B}{2\pi v_-} \right) \right] &= \left[\frac{\hat{\Omega}_{\text{Rot}} \cdot \hat{B} f}{(\hat{\Omega}_{\text{Rot}} \cdot \hat{B} f)_O} - 1 \right] \\ \Rightarrow \frac{\Omega_{\text{Rot}} B \Phi_b}{2\pi c \rho_b} \left[\left(\frac{\rho_+}{\rho_b} \right)_O \left(\frac{v_{+,O}}{v_+} \right) + \left(\frac{\rho_-}{\rho_b} \right)_O \left(\frac{v_{-,O}}{v_-} \right) \right] &= \left[\frac{\hat{\Omega}_{\text{Rot}} \cdot \hat{B} f}{(\hat{\Omega}_{\text{Rot}} \cdot \hat{B} f)_O} - 1 \right] \\ \Rightarrow - \left[\left(\frac{\rho_+}{\rho_b} \right)_O \left(\frac{v_{+,O}}{v_+} \right) + \left(\frac{\rho_-}{\rho_b} \right)_O \left(\frac{v_{-,O}}{v_-} \right) \right] &= \left[\frac{\hat{\Omega}_{\text{Rot}} \cdot \hat{B} f}{(\hat{\Omega}_{\text{Rot}} \cdot \hat{B} f)_O} - 1 \right]\end{aligned}$$

The pair plasma is neutral at point ‘O’ which translates to the condition

$$\rho_{-,O} = -\rho_{+,O} \quad (\text{F12})$$

This gives us the following expression,

$$\left(\frac{\rho_+}{\rho_b} \right)_O \left[\frac{v_+ v_{-,O} - v_- v_{+,O}}{v_+ v_-} \right] = \left[\frac{\hat{\Omega}_{\text{Rot}} \cdot \hat{B} f}{(\hat{\Omega}_{\text{Rot}} \cdot \hat{B} f)_O} - 1 \right]$$

Making use of the fact that the secondary plasma particles are highly relativistic we can reduce the above expression to the form

$$\begin{aligned}\frac{v_+ - v_-}{c} &\approx \left(\frac{\rho_b}{\rho_+} \right)_O \left[\frac{\hat{\Omega}_{\text{Rot}} \cdot \hat{B} f}{(\hat{\Omega}_{\text{Rot}} \cdot \hat{B} f)_O} - 1 \right] \\ \Rightarrow |\Delta\beta| &\approx \left| \left(\frac{\rho_b}{\rho_+} \right)_O \left[\frac{\hat{\Omega}_{\text{Rot}} \cdot \hat{B} f}{(\hat{\Omega}_{\text{Rot}} \cdot \hat{B} f)_O} - 1 \right] \right| \quad (\text{F13})\end{aligned}$$

We call the ratio $(\rho_b/\rho_s) = 1/\kappa_{\text{GJ}}$ as the density term. We call the term in square brackets as the geometrical term. The correction ‘ $f_{\text{Rot}} \approx 1 + O(\Omega^2 r^2/c^2)$ ’ due to rotation can be taken to be 1, as the higher order term $O(\Omega^2 r^2/c^2) \sim 0.01$ at $r = 50R_{\text{NS}}$ for a pulsar with $P = 1$ second. It can be seen that the separation of the electron-positron distribution function is a product of two terms viz., the density term $(\rho_b/\rho_s)_O$ and the geometrical term $[(\hat{\Omega}_{\text{Rot}} \cdot \hat{B})_A / (\hat{\Omega}_{\text{Rot}} \cdot \hat{B})_O - 1]$. The geometrical factor is zero only for very straight magnetic field lines. Thus curved magnetic field line is a necessary requirement of longitudinal drift/ separation of e^\pm distribution in a secondary plasma. [Rahaman et al. 2020](#) used the model by [Gil et al. 2002](#) and found a wide parameter space for the separation of plasma distribution functions exists which depends on the arrangement of non-dipolar surface magnetic field.

APPENDIX G: COMBINING LORENTZ FACTOR

Let the moving frame of reference (MFR) and the plasma frame of reference (PFR) move with respect to the observer's frame of reference (OFR) with beta factor β_{MFR} and β_s in the outward direction along the open magnetic field lines. Let γ_{MFR} and γ_s be the corresponding Lorentz factor in OFR. Let β_{gr} be the beta factor of MFR with respect to PFR, then we have

$$\beta_{\text{gr}} = \frac{\beta_{\text{MFR}} - \beta_s}{1 - \beta_{\text{MFR}}\beta_s} \quad (\text{G1})$$

The Lorentz factor γ_{gr} corresponding to β_{gr} is given by

$$\gamma_{\text{gr}} = \frac{1}{\sqrt{1 - \beta_{\text{gr}}^2}} \quad (\text{G2})$$

Substituting equation (G1) into equation (G2) we get,

$$\gamma_{\text{gr}} = \frac{\gamma_{\text{MFR}}}{2\gamma_s} \quad (\text{G3})$$

which on being re-arranged gives us

$$\gamma_{\text{MFR}} = 2\gamma_s\gamma_{\text{gr}} \quad (\text{G4})$$

In the the ultra-relativistic limit $\gamma_{\text{gr}} = \sqrt{1 + p_{\text{gr}}^2} \approx p_{\text{gr}}$ and the expression reduces to the form

$$\gamma_{\text{MFR}} \approx 2\gamma_s p_{\text{gr}} \quad (\text{G5})$$

APPENDIX H: NOTATIONS AND SYMBOLS USED THROUGHOUT THE TEXT.

- NLD: Non-linear Landau damping.
- GVD: Group-velocity dispersion.
- CNL: Cubic non-linearity.
- κ : Multiplicity of pair plasma. The ratio of the number density of the pair plasma to the co-rotational Goldreich-Julian number density.
- OFR: The observer's frame of reference. Can be identified with co-rotating frame of reference for normal period pulsars.
- PFR: Plasma frame of reference. The frame of reference where the mean velocity of the plasma particles is zero.
- v_{gr} : group velocity of linear Langmuir waves in PFR.
- MFR: Moving frame of reference that moves with velocity v_{gr} with respect to PFR.
- $f_{\alpha}^{(0)}$: plasma particle distribution function (DF) of the α -th species. Two-representative DF viz., a short-tailed Gaussian distribution DF and a long-tailed Lorentzian DF are used.
- p : Dimensionless momentum of plasma particles.
- p_{α} : The mean momentum of the α -th species.
- p_{ph} : Dimensionless momentum corresponding to wave phase velocity.
- p_{gr} : Dimensionless momentum corresponding to wave group velocity.
- σ : width ("temperature") of the Gaussian distribution function.
- Δp : width ("temperature") of the Lorentzian distribution function.
- E : Envelope electric field governed by the non-linear Schrödinger equation along with non-linear Landau damping..
- G : coefficient of the group velocity dispersion.
- q : coefficient of cubic non-linearity.
- s : coefficient of non-linear Landau damping term.
- G_{d} : dimensionless group velocity dispersion.
- q_{d} : dimensionless cubic non-linearity.
- s_{d} : dimensionless non-linear Landau damping term.
- Q : equals $2q_{\text{d}}/G_{\text{d}}$. Decides the typical timescale associated with the emergence of solitons ($\mathcal{O}(1/Q)$)
- ω_{p} : characteristic plasma frequency of Langmuir waves in PFR.
- l : Characteristic length of the linear Langmuir waves in PFR.
- θ : Ratio of the spatial extent of the Langmuir envelope to the characteristic length l of the linear Langmuir waves.
- OFR: Observer's frame of reference. Identified with the co-rotating frame of reference.
- γ_s : Bulk Lorentz factor of the PFR with respect to OFR.